ACS Sustainable Chemistry & Engineering

pubs.acs.org/journal/ascecg

Research Article

Unraveling a Biomass-Derived Multiphase Catalyst for the Dehydrogenative Coupling of Silanes with Alcohols under Aerobic Conditions

Iván Sorribes,* David Ventura-Espinosa, Marcelo Assis, Santiago Martín, Patricia Concepción, Jefferson Bettini, Elson Longo, Jose A. Mata, and Juan Andrés

Cite This: *ACS Sustainable Chem. Eng.* 2021, 9, 2912−2928

Read Online

ACCESS | Metrics & More | Article Recommendations | Supporting Information

ABSTRACT: Herein, a novel silver and chromium nanostructured N-doped carbonaceous material has been synthesized by a biomass-annealing approach using readily available chitosan as a raw material. The resulting catalyst AgCr@CN-800 has been applied for the dehydrogenative coupling reaction of various silanes with different alcohols to obtain the corresponding silyl ethers under aerobic and mild conditions. Besides excellent activity and selectivity, the as-prepared catalyst exhibits good stability and reusability. Characterization by X-ray diffraction, X-ray photoelectron spectroscopy, inductively coupled plasma mass spectrometry, and high-resolution transmission electron microscopy (TEM) in combination with careful examination of the structure with Cs-corrected high-angle annular dark-field scanning TEM revealed that the catalyst AgCr@CN-800 comprises Ag- and CrN-aggregated particles, as well as highly dispersed Ag−N_x and Cr−N_x sites embedded in N-doped graphitic structures. A comparative catalytic study using structure-related catalysts in combination with acid-leaching treatments has shown that the most active species are the Ag particles and that their activity is boosted by the presence of Cr-derived species. By in situ Raman spectroscopy experiments, it has been found that the dehydrogenative coupling of silanes with alcohols in the presence of catalyst AgCr@CN-800 takes place through an oxygen-assisted mechanism.

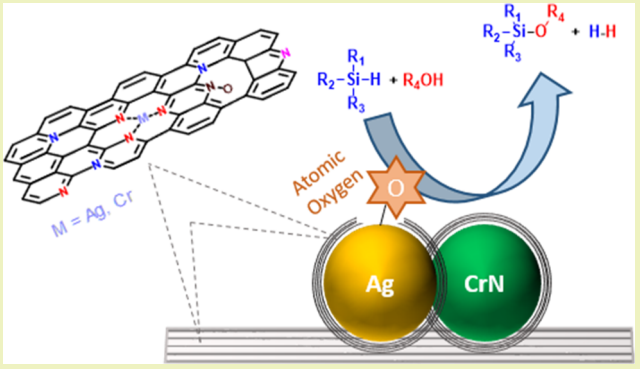

KEYWORDS: *chitosan, silanes, alcohols, dehydrogenative coupling, silyl ethers, oxygen activation, in situ Raman spectroscopy*

INTRODUCTION

Silyl ethers are valuable raw materials in the silicon industry as well as important commodity reagents and protecting groups for alcohols in organic synthesis on laboratory scale.[1−5] In addition, these compounds have also attracted the attention of scientists from the perspective of material science because of their use as reagents for surface coating and modification,[6−13] as well as for the preparation of hybrid organic−inorganic materials.[14−16]

Traditionally, silyl ethers have been synthetized by reaction of halosilanes with alcohols in the presence of a base, thus resulting in the formation of stoichiometric amounts of undesired halide salts.[17−20] In this context, the catalytic dehydrogenative coupling of hydrosilanes with alcohols represents a more atom-economical and hence a more environment-friendly synthetic route.[21,22] Advantageously, since hydrogen is the only generated byproduct, this reaction is also relevant for H_2 generation. In fact, the system based on alcohol/silane pairs has been considered as a potential liquid organic hydrogen carrier that releases H_2 at low temperatures.[23,24] However, although this coupling reaction is thermodynamically favored, the presence of a catalyst is required to improve the reaction kinetics under mild conditions.

To date, a wide variety of transition-metal-based complexes,[25−36] alkaline earth metals,[37] and alkali metal bases[38,39] have been reported as catalysts for the dehydrogenative coupling of hydrosilanes with alcohols. Moreover, metal-free boron-based Lewis acids[40−43] and N-heterocyclic carbenes[44] have also efficiently catalyzed this reaction. Nevertheless, despite good activity and selectivity toward the production of silyl ethers achieved by these catalysts, the use of reusable

Received: December 9, 2020
Revised: January 18, 2021
Published: February 8, 2021

https://dx.doi.org/10.1021/acssuschemeng.0c08953
ACS Sustainable Chem. Eng. 2021, 9, 2912−2928

Scheme 1. Synthesis of Heterobimetallic Materials AgCr@CN-*X* (*X* = 400−900 °C) Used as Catalysts

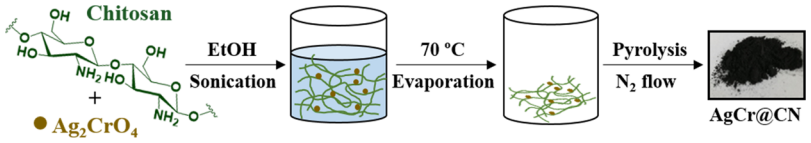

heterogeneous systems is more advantageous from an environmental point of view.

In recent times, with the aim of dealing with global challenges related to sustainability, the scientific community has paid much attention toward the use of metal nanoparticles (NPs) modified by N-doped carbon as catalysts for innovative organic synthesis because of their good activity and controllable selectivity.[45] Different strategies have been developed for the preparation of this kind of nanostructured materials.[46] Among them, the in situ formation of both metal NPs and the N-doped graphitic material is a well-established methodology. Here, non-volatile molecularly defined metal−amine ligated complexes impregnated on different supports,[47−81] metal−organic frameworks,[82−92] or coordination polymers[93−95] are typically used as self-sacrificial templates to obtain metal NPs embedded in a carbonaceous matrix after pyrolysis under an inert gas.

Alternatively, in order to avoid the use of sophisticated organic ligands and synthetically demanding routes of sacrificial template materials, pyrolysis of renewable and available biomass in combination with metal salts represents a more practical catalyst preparation approach.[96−105] In this respect, the natural biopolymer chitosan, which is obtained from industrial fishery biowaste by deacetylation of shrimp or crab shell-derived chitin, is especially useful.[106] Chitosan has been proposed as an attractive precursor for obtaining N-doped carbon materials.[107−122] In addition, its particular structure containing amino- and hydroxyl-coordinating groups has made possible its application as a chelating agent for transition metals.[123−128]

Taking advantage of these properties of chitosan, García and coworkers synthesized Cu NPs supported on N-doped graphene by first preparing a homogeneous solution of Cu salt and chitosan, followed by pyrolysis and sonication.[129] Later, the same group developed a series of facet-oriented Cu_2O,[130−132] Au,[133] Pt,[134] and Ag[135] NPs on (N-doped) graphene films prepared by pyrolysis of nanometer-thick films of chitosan embedding the corresponding transition metal salt and deposited on a quartz substrate. Importantly, a variation or even a complete removal of the N content was reported depending on the pyrolysis temperature and metal nature. Meanwhile, Beller and coworkers prepared Co-based N-doped carbon heterogeneous catalysts by using an adapted synthetic methodology, in which chitosan acts as a solid adsorbent for transition metals instead of being used in solution before pyrolysis.[136−139] In addition to these seminal works, other catalytic materials synthesized following a similar preparation approach have also been reported.[140−149]

In general, metal-based materials prepared by pyrolysis tend to be heterogeneous in composition and particle size. In fact, the resulting materials are typically constituted by metal species of different nature, such as metallic and/or metal oxide NPs. Moreover, the formation of isolated single-atom sites (ISAS) is also feasible when using supports or self-sacrificial templates that have a strong coordination ability with metal atoms.[150−158] Concretely, this is the case of chitosan, in which its unique structure containing amino- and hydroxyl-coordinating groups can promote the formation of ISAS embedded in the N-doped carbon matrix besides other multiple metal species formed by agglomeration during uncontrolled pyrolysis.[159,160] This heterogeneity in chitosan-derived N-doped carbon-based materials makes challenging the identification of active species when they are used in catalysis; however, it is an essential task for future development of catalysts with enhanced efficiency.

With regard to the use of heterogeneous catalysts for the dehydrogenative coupling reaction of hydrosilanes with alcohols, among various available heterogeneous systems,[36,161−179] metal catalysts modified by (doped) graphitic carbon have shown promising results. Cu NPs supported on doped (-boron and/or -nitrogen) graphene,[129] Cu_2O,[130] or Ag[135] facet-oriented nanoplatelets on graphene films, as well as, atomically dispersed Co species anchored on ultrathin two-dimensional N-doped carbon[180] have been proved to be active catalysts for the title reaction. In addition, the use of a metal-free hierarchically porous N and S co-doped carbon is also noteworthy.[181] Despite these findings, the relatively high temperature, long reaction times, the need to perform the reaction under inert atmosphere, and/or the difficulty of preparing catalysts with higher metal loading offer room for improvement.

In this contribution, we report the preparation of a N-doped carbonaceous heterobimetallic nanostructured material by pyrolysis of silver chromate (Ag_2CrO_4) highly dispersed on the readily available biowaste polymer chitosan. We show that the resulting material, which comprises a heterogeneous composition of metal species, efficiently catalyzes the dehydrogenative coupling of hydrosilanes with alcohols under aerobic and mild conditions (even at 0 °C) with excellent selectivity toward the formation of silyl ethers and molecular hydrogen. On the basis of a comparative catalytic study, we demonstrate that the catalytic activity mainly arises from the Ag particles and that their activity is boosted by the presence of Cr-derived species. Furthermore, in situ Raman spectroscopic studies have allowed the explanation of the enhanced catalytic activity, which is directly related to the oxygen activation ability of the catalyst.

RESULTS AND DISCUSSION

Preparation and Catalytic Performance of Catalysts AgCr@CN. We started our study by preparing a series of silver and chromium bimetallic catalysts according to the procedure depicted in Scheme 1. A mixture of chitosan and Ag_2CrO_4 was homogeneously dispersed in ethanol by sonication. After solvent evaporation under atmospheric pressure and continuous stirring conditions, the resultant powder was pyrolyzed at different temperatures in the range from 400 to 900 °C under a nitrogen flow to yield the heterobimetallic materials AgCr@CN-*X*, where *X* stands for the pyrolysis temperature (see the Experimental Section for more preparation details). The metal

https://dx.doi.org/10.1021/acssuschemeng.0c08953
ACS Sustainable Chem. Eng. 2021, 9, 2912−2928

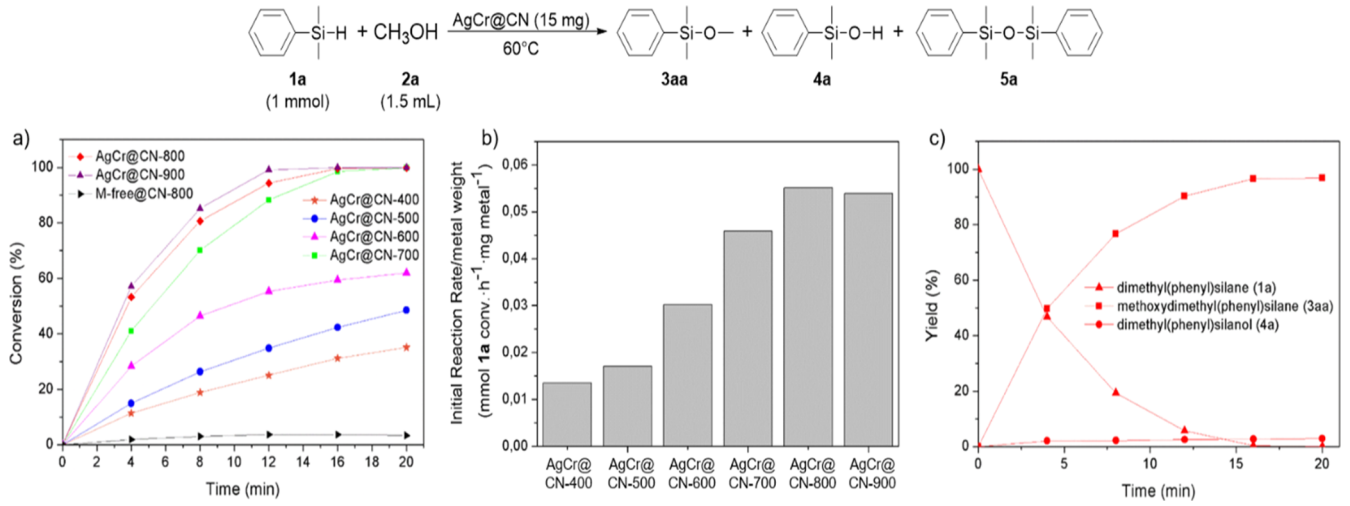

Figure 1. (a) Catalytic performances of catalysts AgCr@CN-*X* (*X* = 400−900) and M-free@CN-800 for the dehydrogenative coupling reaction of **1a** with methanol. (b) Comparison of the metal mass activity. (c) Concentration/time diagram for catalyst AgCr@CN-800.

content in the as-prepared materials was determined by inductively coupled plasma mass spectrometry (ICP−MS) analysis. The obtained results revealed an increase of the metal amount (Ag + Cr) from 13.7 to 18.0 wt % with the pyrolysis temperature because of increasing weight loss in chitosan decomposition (Table S1). Interestingly, the Ag/Cr ratio is maintained constant independent of the pyrolysis temperature.

With these materials in hand, we evaluated their catalytic performance for the dehydrogenative coupling of hydrosilanes with alcohols using as a benchmark system the reaction between dimethyl(phenyl)silane (**1a**) and methanol (**2a**) at 60 °C under aerobic conditions. As shown in Figure 1a, all prepared heterobimetallic materials displayed catalytic activity with excellent selectivity toward the formation of methoxydimethyl(phenyl)silane (**3aa**) (see also Figure S1). A control experiment revealed that no reaction took place in the presence of a metal-free catalyst (M-free@CN-800) prepared by pyrolysis of chitosan at 800 °C in the absence of Ag_2CrO_4, thus indicating that the catalytically active species are metal-based. The most active catalyst, determined by comparison of the initial reaction rates normalized to the mass of metal weights (Figure 1b), resulted to be the heterobimetallic material pyrolyzed at 800 °C (AgCr@CN-800). Other heterobimetallic catalysts containing silver and a second transition metal different from chromium (W or V), which were also prepared following the same preparation methodology shown in Scheme 1, displayed lower activity for the investigated reaction (Figure S2).

In the presence of the most active catalyst AgCr@CN-800 (15 mg; 2.75 mol % of metal with respect to **1a**), full conversion of **1a** was achieved in 20 min, affording **3aa** in 97% yield with only residual amounts (<3%) and traces (<1%) of the corresponding silanol (**4a**) and disiloxane (**5a**) compounds as byproducts, respectively (Figure 1c). Moreover, H_2 release was also detected during the reaction between **1a** and **2a**. This dehydrogenative coupling reaction also proceeds well when using lower amounts of catalyst AgCr@CN-800 (5 mg; 0.91 mol % of metal with respect to **1a**), corresponding to a turnover number of 111. Interestingly, the reaction could also be conducted at lower temperature, 30 °C and even 0 °C, achieving full conversion of **1a** with excellent selectivity to **3aa** in 1 and 2 h, respectively (Figure S3), together with the formation of equimolecular amounts of H_2 (see the Supporting Information). It is worth mentioning that compared to previously reported Ag-based heterogeneous systems, the catalyst AgCr@CN-800 catalyzes this reaction at significant lower temperatures (0 °C).[135,172,182−185]

Interestingly, the reaction rate was significantly increased when pure O_2 was bubbled into the reaction solution, providing a 98% yield of **3aa** within 20 min at 30 °C (TOF = 327 h^{-1}). In contrast, almost no reaction took place when the reaction was carried out under Ar atmosphere, thus revealing that the presence of the catalyst AgCr@CN-800 in combination with O_2 is essential to achieve the dehydrogenative coupling reaction of **1a** with methanol (Figure S3).

Characterization of Catalyst AgCr@CN-800. The best heterobimetallic material AgCr@CN-800 in terms of catalytic activity was characterized in detail. The X-ray diffraction (XRD) pattern (Figure 2) is dominated by the presence of

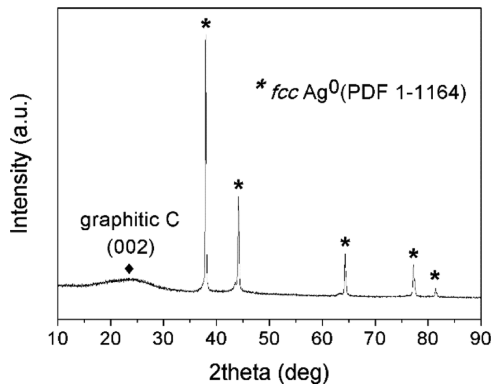

Figure 2. XRD pattern for catalyst AgCr@CN-800.

diffraction peaks associated with the face-centered cubic structure of Ag^0 in agreement with the JCPDS database (PDF card 1-1164). Since these peaks are very sharp, it is expected that this phase is present in the form of large particles. Moreover, a broad shoulder peak in the range of 20−30° (2θ) associated with reflections of the (002) plane of graphitic carbon could also be inferred.[186] However, no

https://dx.doi.org/10.1021/acssuschemeng.0c08953
ACS Sustainable Chem. Eng. 2021, 9, 2912−2928

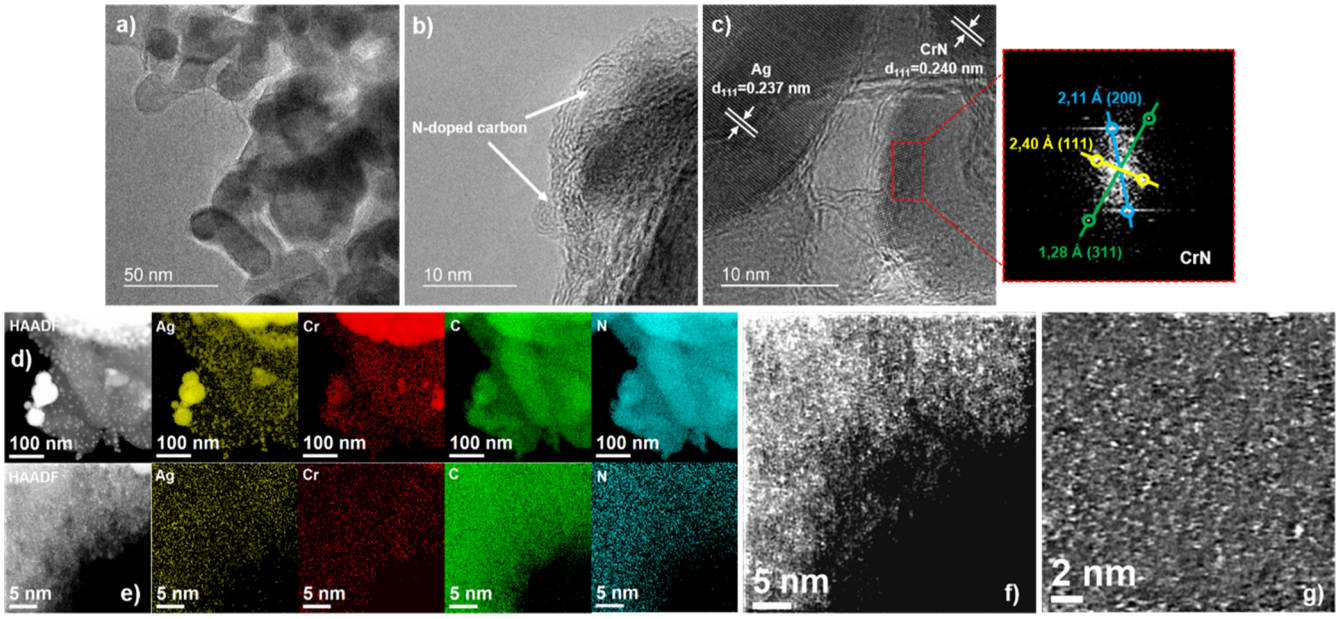

Figure 3. Electron microscopy characterization of catalyst AgCr@CN-800. TEM (a) and HRTEM (b,c) micrographs. The inset shows the FFT from the square region in image (c). (d,e) HAADF−STEM images and EDS elemental mapping of Ag, Cr, C, and N. (f,g) High-magnification images for the Cs-corrected HAADF−STEM analysis.

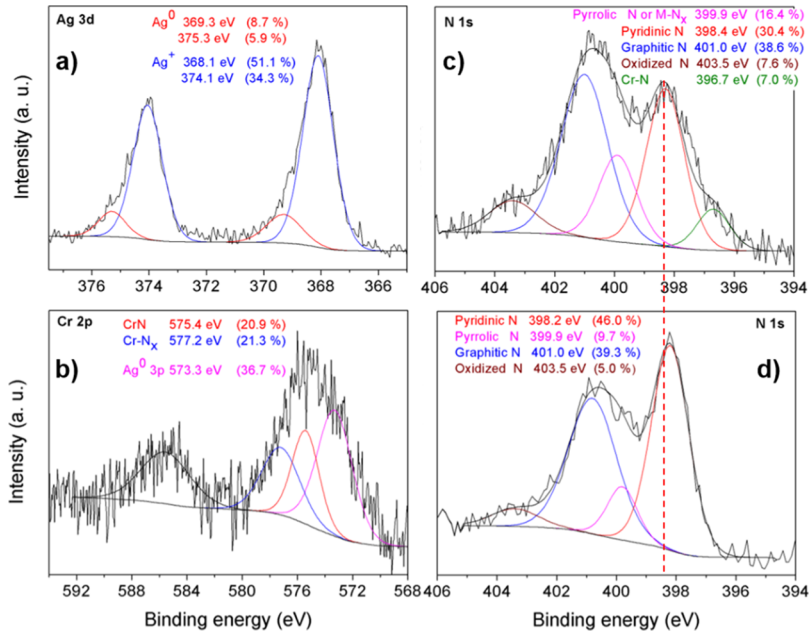

Figure 4. XPS spectra of Ag 3d (a), Cr 2p (b), and N 1s (c) core levels of catalyst AgCr@CN-800. (d) N 1s XPS spectrum of catalyst M-free@CN-800.

additional peaks corresponding to chromium species were detected.

Transmission electron microscopy (TEM) images show aggregates of metal particles with non-homogeneous sizes of tens to hundreds of nanometers. This broad site distribution is likely generated by partial metal agglomeration during the pyrolysis treatment because of the high metal content (Figures 3a and S4). The high-resolution TEM (HRTEM) images show two types of metal particles of different nature, both coated by few layers of a (defect/N-doped) graphitic carbon shell (Figure 3b,c). The well-resolved lattice spacing of 0.237 nm consistent with the (111) plane of the cubic Ag phase was clearly identified in some of these particles. Besides, an additional phase of chromium nitride (CrN) that displays the characteristic lattice spacing of 0.239 nm associated with its (111) plane was also detected in the HRTEM images. Moreover, the nature of these particles was undoubtedly confirmed by a fast Fourier transform (FFT) analysis, which revealed other characteristic lattice fringe spaces of 0.211 and 0.128 nm associated with the (200) and (311) planes of CrN, respectively (Figure 3c, inset).

Spherical aberration (Cs)-corrected scanning TEM (STEM) using a high-angle annular dark-field (HAADF) detector coupled with spectroscopic analysis by means of energy-dispersive X-ray spectroscopy (EDS) was employed to

https://dx.doi.org/10.1021/acssuschemeng.0c08953
ACS Sustainable Chem. Eng. 2021, 9, 2912−2928

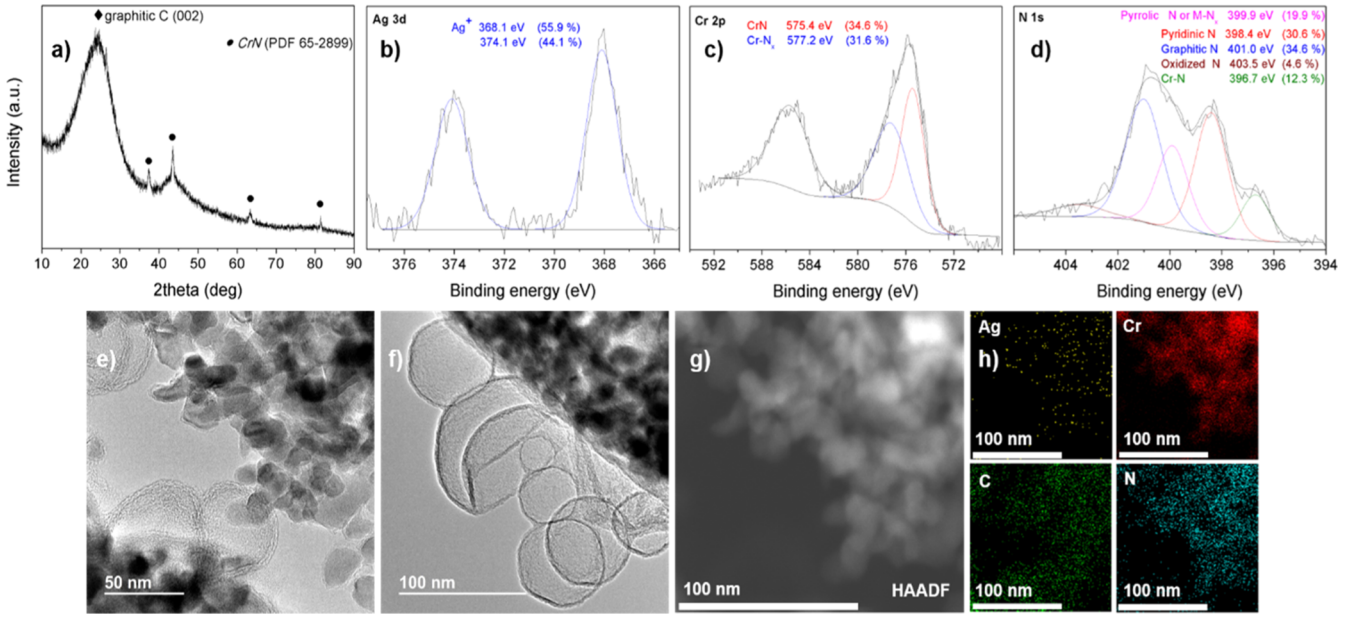

Figure 5. Characterization of catalyst AgCr@CN-800-acid. (a) XRD spectrum. Ag 3d (b), Cr 2p (c), and N 1s (d) core-level XPS spectra. TEM (e,f) and HAADF-STEM (g) images. (h) EDS elemental mapping of Ag, Cr, C, and N.

investigate the structure of catalyst AgCr@CN-800 in a further extent. These studies revealed that Ag, Cr, N, and C elements overlap in spatial locations on each other around the entire sample, including particles (Figures 3d and S5) as well as sites where no particles were visualized (Figures 3e and S5), thus suggesting that metal species may be atomically distributed along the N-doped graphitic material. Interestingly, a closer look at these regions revealed a high density of monodispersed bright dots, likely associated with highly dispersed metal atoms of both Ag and Cr, according to the EDS elemental mapping analysis results (Figures 3f,g, S6, and S7).

For further characterization of the catalyst surface, X-ray photoelectron spectroscopy (XPS) measurements were performed. The high-resolution Ag 3d core-level spectrum displays two peaks at ~368 and 374 eV associated with the characteristic spin−orbit splitting of Ag $3d_{5/2}$ and Ag $3d_{3/2}$ orbitals, respectively, each of them being possible to be fitted into two separated components denoting the presence of two distinct chemical Ag species (Figure 4a). More specifically, the components at 368.1 and 374.1 eV correspond to Ag^+ species, whereas the ones at 369.3 and 375.3 eV are related to metallic Ag.[187−191] The higher contribution of the component associated with Ag^+ species suggests that, in spite of the shielding effect of thick N-doped graphitic carbon layers encapsulating the Ag particles, these could be constituted by a metallic core and a partially oxidized surface. In addition, it should be considered that the XPS-detectable Ag^+ species could also arise from highly dispersed Ag^+ species inserted in the graphitic sheets coordinated to N atoms, that is, as AgN_x sites. Comparison of the obtained electron binding energy of Ag $3d_{5/2}$ (368.1 eV) in catalyst AgCr@CN-800 with that for previously reported molecular defined complexes that contain Ag−N bonds within a related structure (368.4 eV)[192] revealed a prominent increase of the electron density of the Ag^+ species in the graphitized structure, in good agreement with previous studies.[150]

Determination of Cr-oxidation states in heterobimetallic materials containing Ag is challenging because in the Cr 2p region of the XPS spectrum, some Cr species have similar electron binding energy values than that of the Ag 3p peak (~573.6 eV) associated with metallic Ag. The Cr 2p XPS spectrum (Figure 4b) for catalyst AgCr@CN-800 shows a broad peak, which could be fitted into three different components after deconvolution. The major peak at 573.3 eV can be ascribed to metallic Ag, whereas according to the literature, the other two peaks at 575.4 and 577.2 eV denote the presence of CrN[193] and atomically dispersed Cr−N_x sites embedded in the graphitic sheets,[194] respectively.

The signal deconvolution in the high-resolution N 1s energy-level spectrum (Figure 4c) suggests that catalyst AgCr@CN-800 contains different nitrogen species, at least including pyridinic N-oxide (403.5 eV), graphitic-N (401.0 eV), pyrrolic-N (399.9 eV), and pyridinic-N (398.4 eV). Furthermore, an additional component (at 396.7 eV) attributed to CrN could also be inferred, which is absent in the XPS spectrum of the metal-free catalyst M-free@CN-800 (Figure 4d). Importantly, further comparison of both spectra (Figure 4c,d) revealed that while the relative content of graphitic-N and pyridinic N-oxide species is almost the same, an increase of the ratio of pyrrolic-N to pyridinic-N species is observed in catalyst AgCr@CN-800. This increase could be associated with the presence of highly dispersed species attached to pyridinic-N that results in the formation of M−N_x (M = Ag and Cr) sites, whose binding energies fall in the same range as the pyrrolic-N function binding energy. Moreover, an energy shift of over 0.2 eV was detected in the pyridinic-N component of catalyst AgCr@CN-800, thus verifying the existence of metal−N interactions.[150,152,195]

Acid Leaching and Characterization of Catalyst AgCr@CN-800-Acid. Catalyst AgCr@CN-800 was leached with acid (see details in the Experimental Section) and further characterized. The Ag and Cr contents, determined by ICP−MS analysis, in the leached catalyst (denoted as AgCr@CN-800-acid) were reduced from 12.74 to 0.12 and from 3.74 to 2.29 wt %, respectively. In consequence, no diffraction peaks associated with metallic Ag species were detected in the XRD

https://dx.doi.org/10.1021/acssuschemeng.0c08953
ACS Sustainable Chem. Eng. 2021, 9, 2912−2928

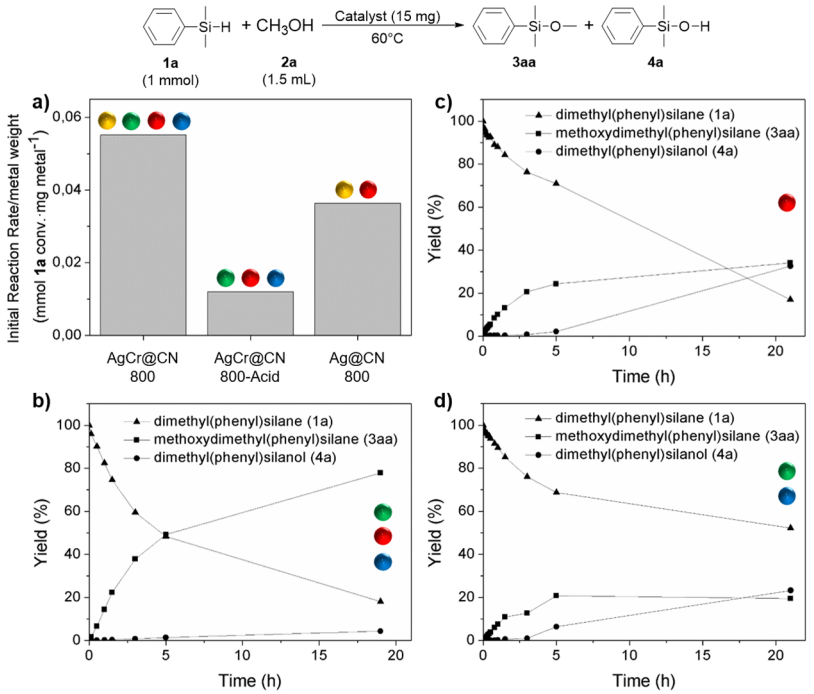

Figure 6. (a) Comparison of the metal mass activity for catalysts AgCr@CN-800, AgCr@CN-800-acid, and Ag@CN-800 in the dehydrogenative coupling reaction of **1a** with methanol (**2a**). Concentration/time diagram for catalyst AgCr@CN-800-acid (b), Ag@CN-800-acid (c), and Cr@CN-800-acid (d). Reaction conditions: **1a** (1 mmol), **2a** (1.5 mL), catalyst (15 mg), and 60 °C. Colored dots represent which active species are present in the catalyst used: Ag particles (yellow), CrN particles (green), AgN_x sites (red), and CrN_x sites (blue).

pattern of the acid-leached catalyst AgCr@CN-800-acid (Figure 5a). However, besides the broad diffraction peaks of graphitic carbon (at 2θ values of 25.3 and 43.6°), other peaks located at 37.5, 43.6, 63.4, and 76.1°, which could be indexed to the (111), (200), (220), and (311) planes, respectively, of the cubic phase of CrN (PDF card 65-2899), became known in catalyst AgCr@CN-800-acid. This confirms that the acid-leaching treatment fully removed the Ag particles, while keeping the CrN phase almost intact, which is known to display an excellent chemical stability to acids.[196,197]

The diffraction peaks associated with CrN are also present in the XRD pattern measured after the acid treatment of a catalyst (AgCr@CN-800-Ar) pyrolyzed under Ar atmosphere instead of using N_2 (see Figure S8). This result, besides the fact that only a slight decrease of the N content (determined by combustion elemental analysis) was detected in catalyst AgCr@CN-800-Ar (7.6 wt %) when compared with catalyst AgCr@CN-800 (7.8 wt %), proves that the CrN phase is preferentially formed during the pyrolysis treatment by extracting N atoms from chitosan rather than by activation of N_2 gas molecules. Moreover, both catalysts AgCr@CN-800 and AgCr@CN-800-Ar displayed similar catalytic performance for the investigated dehydrogenative coupling reaction between dimethylphenylsilane (**1a**) and methanol (see Figure S8).

Morphological characterization of the acid-etched catalyst AgCr@CN-800-acid by TEM showed the presence of coated NPs (~30 nm) as well as hollow-centered (defect/N-doped) graphitic carbon layers (Figure 5e,f). These empty carbonaceous spheres result from the leaching of Ag particles, further confirming the core−shell structure of this heterobimetallic material. The elemental distribution of catalyst AgCr@CN-800-acid was investigated by EDS elemental mapping (Figure 5g,h) and confirms that, as in the case of catalyst AgCr@CN-800, Cr, C, and N elements overlap well in spatial locations, while monodispersed Ag is present in a considerably lower amount, in good agreement with the ICP−MS analysis.

Interestingly, the Ag 3d core-level XPS spectrum of catalyst AgCr@CN-800-acid discloses the only presence of Ag^+ ionic species (i.e., AgN_x sites) represented as two peaks with electron-binding energy values of 368.1 and 374.1 eV after deconvolution and fitting (Figure 5b). It should be noted that the component associated with the Ag 3p peak (~573.6 eV) of metallic Ag completely disappeared from the Cr 2p core-level XPS spectrum (Figure 5c), being possible to fit the observed peak into two only components corresponding to CrN (575.4 eV) and to atomically dispersed Cr−N_x sites embedded in the graphitic carbon (577.2 eV). On the contrary, no relevant changes are observed in the high-resolution N 1s energy-level spectrum after the acid-leaching treatment (Figure 5d).

Based on all characterization results before and after the acid-leaching treatment, we can conclude that catalyst AgCr@CN-800 is a heterobimetallic N-doped carbonaceous material, in which different metal species coexist. More specifically, catalyst AgCr@CN-800 comprises Ag- and CrN-aggregated particles covered by few layers of defect N-doped graphitic carbon containing highly dispersed Ag−N_x and Cr−N_x species as well.

Probing into the Metal Active Species. To unveil which of these species is catalytically active for the investigated dehydrogenative coupling reaction between dimethylphenylsilane (**1a**) and methanol (**2a**) to afford methoxydimethyl(phenyl)silane (**3aa**), the titled reaction was carried out in the presence of different catalysts (see the Experimental Section and the Supporting Information for preparation and characterization details, respectively). As shown in Figure 6a, a significant decrease of the initial reaction rate (normalized to the mass of metal weights) was achieved by using the acid-

https://dx.doi.org/10.1021/acssuschemeng.0c08953
ACS Sustainable Chem. Eng. 2021, 9, 2912−2928

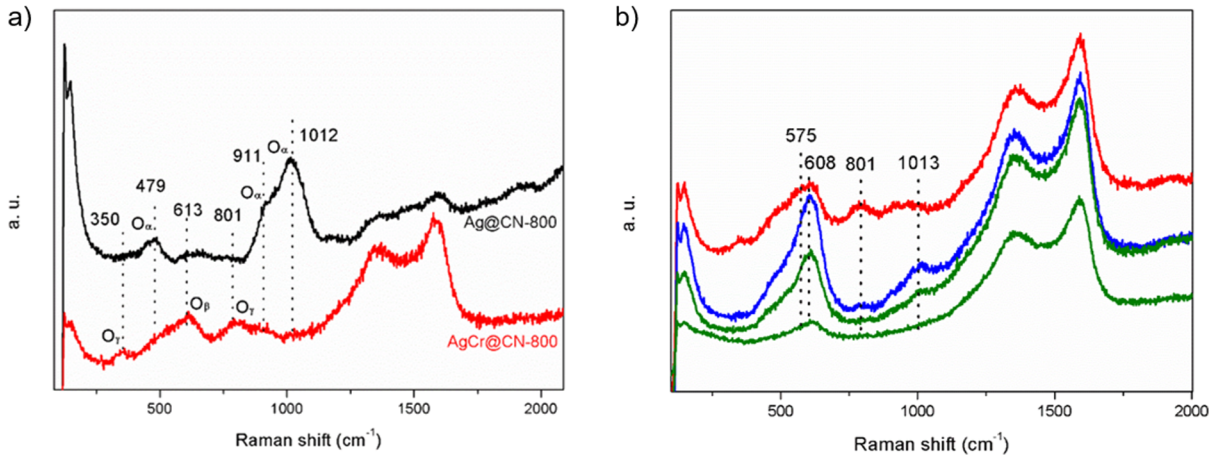

Figure 7. (a) Evolution of the bands in the Raman spectra on catalysts AgCr@CN-800 (red line) and Ag@CN-800 (black line) in a 20% O_2/Ar flow at room temperature. (b) Evolution of the bands in the Raman spectra on catalyst AgCr@CN-800 after sequentially dosing at room temperature a 20% O_2/Ar flow (red line), a methanol/Ar flow (blue line), and a silane **1a**/Ar flow (green lines).

etched catalyst AgCr@CN-800-acid. Nevertheless, it is worth mentioning that reaction proceeded with excellent selectivity after longer reaction times (Figure 6b). Since Ag particles are the species removed with the acid-leaching treatment, this result denotes that they are required for the high activity of catalyst AgCr@CN-800, while the remaining species (i.e., CrN particles and highly dispersed CrN_x and AgN_x sites) contribute in a considerable lower extent to the overall catalytic activity.

In the presence of a monometallic Ag-based catalyst (Ag@CN-800), which is constituted by core−shell metallic NPs with a narrow size distribution (5−20 nm) and by highly dispersed AgN_x species (see Figure S9 and accompanying discussion), good activity toward the formation of product **3aa** was achieved (Figure 6a) as well. However, in spite of the smaller particle size (and therefore higher specific surface area to interact with the reactants), catalyst Ag@CN-800 is less active than the heterobimetallic one AgCr@CN-800 for the investigated reaction. This result unambiguously corroborates that the presence of chromium-derived species in catalyst AgCr@CN-800 boosts its catalytic activity.

When the monometallic catalyst Ag@CN-800 was leached with acid to remove the metallic Ag NPs, and the resulting material (Ag@CN-800-acid) only containing highly dispersed $Ag-N_x$ sites (see Figure S10 and accompanying discussion) was used as a catalyst under otherwise the same conditions, a decrease of the selectivity toward the coupling product **3aa** was observed as the conversion increases (Figure 6c). Similarly, the use of catalyst Cr@CN-800-acid, which is constituted by the same Cr species (i.e., CrN and highly dispersed $Cr-N_x$ sites) than catalyst AgCr@CN-800-acid but in the absence of $Ag-N_x$ species (see Figure S11 and accompanying discussion), led to the same loss of selectivity as well (Figure 6d).

Overall, the above comparative catalytic study reveals that Ag particles are the most active species and that their activity is boosted by the presence of Cr-derived species. In the absence of Ag particles, the rest of metal species (i.e., CrN particles as well as highly dispersed $Ag-N_x$ and $Cr-N_x$ sites) cooperatively catalyze this reaction with a slower reaction rate but with high selectivity. However, a considerable loss of selectivity is achieved when the catalyst only comprises either $Ag-N_x$ sites or Cr-derived species (i.e., CrN particles and $Cr-N_x$ sites), further supporting the synergistic role of Ag- and Cr-derived species in catalyst AgCr@CN-800.

Kinetic and In Situ Raman Spectroscopy Investigations. To get insights into the reaction pathway for the dehydrogenative coupling of silanes with alcohols in the presence of catalyst AgCr@CN-800, kinetic experiments at 30 °C under air conditions were performed by measuring initial reaction rates at variable concentrations of silane **1a** or methanol (**2a**) while keeping the other reactant constant. The initial reaction rate for the generation of **3aa** was proportional to the concentration of methanol, but a decrease was observed when increasing the amount of the silane (Figure S12). According to Hougen−Watson/Langmuir−Hinshelwood principles, developed for describing reaction mechanisms occurring on the surface of heterogeneous catalysts, these observations suggest that the alcohol activation is the rate-determining step and that both reactants, that is, the silane and the alcohol, compete by the same active sites.[198−201] Furthermore, a kinetic isotope effect (k_H/k_D = 2.45) was observed when using O-deuterated methanol (CH_3OD) as a reactant, further confirming that the activation of the O−H bond is involved in the slowest reaction step.

As commented above, the presence of O_2 is crucial to accomplish the dehydrogenative coupling reaction and higher catalytic activity was obtained in the presence of catalyst AgCr@CN-800 in comparison with the Cr-free catalyst (Ag@CN-800). Thus, with the aim of getting more clues into the reaction mechanism, we first performed Raman studies of oxygen activation, revealing that catalyst AgCr@CN-800 displays a higher ability to activate oxygen than catalyst Ag@CN-800 (Figure 7a). Apart from the G- (1570 cm^{-1}), D- (1350 cm^{-1}), and 2D- (2500−2800 cm^{-1}) bands (Figure S13), characteristic of the formation of graphitic carbon with some degree of defect sites, the recorded spectra for both catalysts display different Raman bands as a consequence of a markedly different reactivity toward O_2 activation. The Raman spectrum of catalyst AgCr@CN-800 exhibits intense bands at 613 cm^{-1} corresponding to the subsurface atomic oxygen species (labeled O_β) and at 801 and 350 cm^{-1} associated with the stretching and bending vibration of chemisorbed surface atomic oxygen species (denoted as O_γ).[202−204] In the opposite, in catalyst Ag@CN-800, weakly activated molecular O_2 is predominately observed (Raman bands at 911 and 1012 cm^{-1})[203,205] together with weakly adsorbed atomic oxygen species at 479 cm^{-1} (denoted as Oα). According to previous

https://dx.doi.org/10.1021/acssuschemeng.0c08953
ACS Sustainable Chem. Eng. 2021, 9, 2912−2928

studies on Ag-based catalysts, the different reactivity toward oxygen activation observed between both catalysts could arise from structural defects and/or modification of electronic properties in the Ag particles likely provoked in catalyst AgCr@CN-800 by the presence of Cr species, which are in intimate contact with the Ag particles, as revealed by electron microscopy characterization.

In order to unravel the role of the surface oxygen species on the reaction mechanism, "in situ" Raman experiments in the presence of catalyst AgCr@CN-800 were undertaken. After dosing methanol on a pre-oxidized catalyst, new Raman bands associated with hydroxyl (575 cm^{-1}) and alkoxy (ν(C−O) at 1013 cm^{-1}) species emerged concomitant with the depletion of the bands at 801 cm^{-1} associated with the surface O_γ species (Figure 7b). A similar depletion behavior of these species was also observed after silane dosing on the pre-oxidized catalyst in the absence of methanol (Figure S14a), further confirming that both reactants, that is, the silane and the alcohol, compete by the same active sites, as revealed by the kinetic study. It should be mentioned that the reactivity observed for the surface O_γ species is in line with other studies in the literature where they have been reported as active centers for silane[206−209] and methanol[204] oxidation reactions. Interestingly, no O−H bond activation of methanol was observed in a non-oxidized catalyst surface (Figure S14b). This result agrees not only with the fact that no reaction took place under an inert atmosphere but also with the higher reaction rate observed by bubbling pure O_2 gas into the reaction, which agrees with the kinetic findings where methanol activation was found to be the rate-limiting step.

Next, the reactivity of the pre-formed methoxy (−OCH_3) and hydroxyl (−OH) species was investigated after silane feeding. As shown in Figure 7b, the methoxy species (1012 cm^{-1}) rapidly disappeared in the presence of silane together with a decrease in the intensity of the band associated with hydroxyl and subsurface oxygen species (575−613 cm^{-1}), thus indicating that the reaction between activated methanol and silane to form the silyl ether **3aa** and H_2 was accomplished. The fact that the silanol (**4a**) and disiloxane (**5a**) compounds were detected as byproducts in the macrokinetic studies agrees with the herein observed progressive depletion of the Raman bands at 613 and 801 cm^{-1} associated with subsurface O_β and surface O_γ species, respectively, by further reaction of these species with the silane.

Based on these results, a plausible mechanism for the dehydrogenative coupling of silanes with alcohols in the presence of catalyst AgCr@CN-800 is proposed (Scheme 2). Oxygen-activated Ag surface species act as Brønsted base sites producing hydroxyl and alkoxy species by reaction with the alcohol. No direct evidence on the silane activation on the catalyst surface was obtained likely because it is a fast step of the overall catalytic reaction. However, considering the well-established reactivity of silanes with metals, the activation could take place through the formation of a silyl−metal hydride intermediate by Si−H bond insertion into the Ag surface.[206] Subsequently, the nucleophilic attack of the alkoxy species derived from the alcohol to the electrophilic Si atom of the silyl−metal hydride intermediate would generate the corresponding silyl ether and molecular H_2 as well as the recovering of the oxygen activated Ag surface species. It should be noted that, according to the work of Belkova, Shubina, and coworkers,[210] the silane activation could also be accounted by coordination of the previously formed alkoxide ionic species yielding hypervalent pentacoordinate silicon complexes,[211−213]

Scheme 2. Proposed Mechanism for the Oxygen-Assisted Dehydrogenative Coupling Reaction of Silanes with Alcohols in the Presence of Catalyst AgCr@CN-800

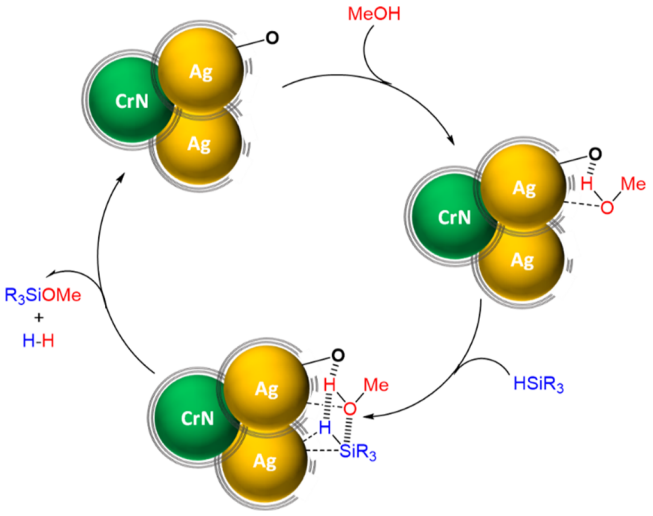

which enable the formation of dihydrogen-bonded (MeO)-R_3SiH···HOMe species, making the proton−hydride transfer and H_2 formation straightforward.

Reusability of Catalyst AgCr@CN-800. In order to investigate the recyclability of catalyst AgCr@CN-800, the model reaction between the silane **1a** and methanol was scaled up by the factor of 7 for practical reasons. After each catalytic run, the catalyst was separated from the reaction mixture, washed with ethyl acetate and diethyl ether, and reused without any reactivation treatment. ICP−MS analysis of the reaction filtrate after each run revealed that the metal (Ag and Cr) content was below the detection limit, thus confirming that no significant metal leaching occurred. Moreover, when the catalyst was removed from the reaction mixture by filtration at 51% yield of **3aa**, the reaction did not proceed any further (Figure S15).

After the fourth run, the morphology of the catalyst was investigated by TEM and EDS elemental mapping (Figure S16). Metal particles were still covered by a few layers of N-doped graphitic carbon shell, and good dispersion of all elements (C, N, Ag, and Cr) overlapping to each other in spatial locations could also be observed. Furthermore, no significant changes were detected by XRD and XPS analyses (Figure S17). The stability of catalyst AgCr@CN-800, suggested by the characterization results, was further confirmed by the excellent yields of the silyl product **3aa** obtained after each catalytic run with only a slight decrease of the reaction rate, which could be overcome by prolonging the reaction time (Figure 8).

Reaction Scope of Catalyst AgCr@CN-800. The catalytic performance of catalyst AgCr@CN-800 was further explored for the dehydrogenative coupling of various silanes with different alcohols. As shown in Table 1, excellent selectivity to the corresponding alkoxysilane products (**3ab**−**ag**) was achieved in the reaction between dimethylphenylsilane (**1a**) and alcohols (**2b**−**g**) with longer alkyl chain length, including linear and branched ones (Table 1, entries 1−7). Compared to methanol, longer reaction times were needed for full (or high) conversions, most likely because of steric effects. Benzyl alcohol (**2h**) also reacted efficiently at higher temperature (100 °C) with silane **1a** affording the desired

https://dx.doi.org/10.1021/acssuschemeng.0c08953
ACS Sustainable Chem. Eng. 2021, 9, 2912−2928

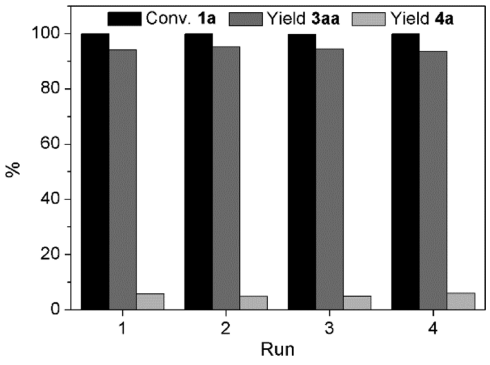

Figure 8. Recycling of catalyst AgCr@CN-800 for the dehydrogenative coupling reaction of **1a** with methanol. Reaction conditions: **1a** (7 mmol), **2a** (10.5 mL), catalyst AgCr@CN-800 (105 mg), 30 °C, 75 min (run 1), 90 min (run 2), 135 min (run 3), or 180 min (run 4). Conversions and yields determined by GC using anisole as an internal standard (380 μL, 3.5 mmol).

Table 1. Dehydrogenative Coupling of Silanes and Alcohols Catalyzed by AgCr@CN-800[a]

entry	silane	alcohol	time [min]	conversion[b] [%]	selectivity to **3**[b] [%]
1[c]	Me_2PhSiH (**1a**)	MeOH (**2a**)	20	>99	97 (89)[d]
2	Me_2PhSiH (**1a**)	EtOH (**2b**)	60	>99	93
3[c]	Me_2PhSiH (**1a**)	*n*-PrOH (**2c**)	60	>99	94
4[e]	Me_2PhSiH (**1a**)	*n*-BuOH (**2d**)	180	96	96
5[c,e]	Me_2PhSiH (**1a**)	*n*-HexOH (**2e**)	60	97	96
6[e]	Me_2PhSiH (**1a**)	*i*-PrOH (**2f**)	60	99	85
7	Me_2PhSiH (**1a**)	*sec*-BuOH (**2g**)	360	99	89
8[e,f]	Me_2PhSiH (**1a**)	BzOH (**2h**)	120	95	95
9	Me_2PhSiH (**1a**)	HOEtOH (**2i**)	60	>99	(79)
10[c]	Ph_3SiH (**1b**)	MeOH (**2a**)	60	95	(93)
11[c]	Ph_2SiH_2 (**1c**)	MeOH (**2a**)	45	99	89
12	Ph_2SiH_2 (**1c**)	*n*-PrOH (**2c**)	45	99	(92)
13	Ph_2SiH_2 (**1c**)	*n*-BuOH (**2d**)	60	99	(80)
14[c,g]	$PhSiH_3$ (**1d**)	MeOH (**2a**)	20	99	89

[a]Reaction conditions: silane (1 mmol), alcohol (1.5 mL), AgCr@CN-800 (15 mg), and 60 °C. [b]Determined by GC using anisole (54 μL, 0.5 mmol) as an internal standard. Yield of isolated products in parentheses. [c]Anhydrous alcohol as a reactant. [d]Isolated yield on a gram-scale reaction: **1a** (1 g), MeOH (11 mL), AgCr@CN-800 (110 mg), 30 °C, and 75 min. [e]AgCr@CN-800 (30 mg). [f]100 °C. [g]AgCr@CN-800 (5 mg).

silyl ether product (**3ah**) in 95% selectivity (Table 1, entry 8). Interestingly, when the reaction was performed in the presence of ethylene glycol (**2i**), the silyloxy(ethan-1-ol) product (**3ai**) was afforded with high selectivity (Table 1, entry 9). Besides silane **1a**, triphenyl- (**1b**), diphenyl- (**1c**), and phenylsilane (**1d**) were also excellent candidates to accomplish the dehydrogenative coupling reaction with different alcohols in the presence of catalyst AgCr@CN-800 to the corresponding mono- (**3ba**), di- (**3ca**, **3cc**, **3cd**), and trialkoxysilane (**3da**) products with good to excellent selectivity (Table 1, entries 10−14). In general, the discrete loss of selectivity is associated with the formation of the corresponding silanol, disiloxane, and/or siloxane oligomer products by reaction of silanes with oxygen activated Ag surface species and/or with ubiquitous water present in alcohols.

CONCLUSIONS

We have developed a series of N-doped carbonaceous heterobimetallic nanostructured materials prepared by pyrolysis of chitosan at different temperatures in the presence of highly dispersed Ag_2CrO_4. Their catalytic potential has been investigated for the dehydrogenative coupling reaction of various silanes with different alcohols. The most active catalyst AgCr@CN-800 catalyzes this reaction under aerobic and mild conditions, even at 0 °C, affording the corresponding silyl ether products with excellent selectivity. Furthermore, the catalyst displays good stability and recyclability.

Characterization results revealed that catalyst AgCr@CN-800 comprises Ag- and CrN-aggregated particles, as well as highly dispersed Ag−N_x and Cr−N_x sites embedded in N-doped graphitic structures. The rational design of structure-related catalysts in combination with acid-leaching treatments allowed for carrying out catalytic control experiments, which revealed that the most active species are the Ag particles and that their activity is boosted by the presence of Cr-derived species. It has been demonstrated by in situ Raman spectroscopy that this boosting effect is related with a higher ability for the generation of oxygen activated surface species, which has resulted to play a crucial role as Brønsted base sites for the dissociative activation of the alcohol that is the rate-determining step of the whole process.

This work not only provides solid evidence of a catalyst involving surface oxygen activated species as key active sites for environmentally benign reactions for green organic synthesis but also offers insights into disentangling the heterogeneous composition of chitosan-derived annealed materials containing metals.

EXPERIMENTAL SECTION

Reagents. Ag_2CrO_4 was synthesized according to the co-precipitation method previously reported in the literature.[214] α-Ag_2WO_4 and α-$AgVO_3$ were prepared according to literature methods as well.[215,216] Chitosan, silanes, and alcohols, including anhydrous methanol, were obtained from commercial sources (Sigma-Aldrich) and were used as received, while *n*-propanol and *n*-hexanol were dried over molecular sieves prior to being used.

Synthesis of Catalyst AgCr@CN. In a 250 mL beaker, Ag_2CrO_4 (0.074 g) and chitosan (0.926 g) were dispersed by sonication in 30 mL of ethanol for 20 min. Then, the solvent was evaporated under atmospheric pressure and stirring conditions at 70 °C, and the residue was dried overnight at this temperature under high vacuum. The dried sample was transferred into a quartz tube, and pyrolyzed at temperatures between 400 and 900 °C for 2 h in a vertical tubular oven with a ramp rate of 10 °C/min while flushing N_2 through the tube constantly until the oven was cooled down to room temperature. The resulting material was ground in an agate mortar and stored in an Eppendorf under air. Catalyst M-free@CN was prepared by directly pyrolyzing chitosan (1 g) under the same annealing treatment, followed by grinding in an agate mortar.

Synthesis of AgW@CN-800 and AgV@CN-800. The preparation of catalysts AgW@CN-800 and AgV@CN-800 was carried following the same procedure to the one described for AgCr@CN materials. α-Ag_2WO_4 (0.070 g) or 0.078 g of α-$AgVO_3$, and 0.930 or 0.922 g of chitosan, respectively, were used as precursors. The other

https://dx.doi.org/10.1021/acssuschemeng.0c08953
ACS Sustainable Chem. Eng. 2021, 9, 2912−2928

experimental procedures were the same, and the pyrolysis temperature was 800 °C.

Preparation of Catalyst AgCr@CN-800-Acid. AgCr@CN-800-acid was prepared by acid leaching of AgCr@CN-800. In a 100 mL beaker, 200 mg of catalyst AgCr@CN-800 was dispersed in a 0.5 mol/L H_2SO_4 aqueous solution (50 mL) under stirring conditions and heated at 75 °C for 6 h. After that, the resulting material was recovered by centrifugation, washed twice with water, twice with ethanol, and dried at 60 °C overnight.

Synthesis of Ag@CN-800. Chitosan (0.924 g) was dispersed by sonication for 20 min in an ethanol solution of $AgNO_3$ (0.076 g in 30 mL). The other experimental procedures were the same as the ones described for AgCr@CN materials, and the pyrolysis temperature was 800 °C.

Synthesis of Ag@CN-800-Acid. Ag@CN-800-acid was prepared by five consecutive acid-leaching treatments starting from 240 mg of catalyst Ag@CN-800. After each treatment, the resulting material was recovered by centrifugation, washed twice with water and twice with ethanol, dried at 60 °C, and used for the next one. The first three acid-leaching treatments were carried out in a 100 mL beaker, in which the catalyst was dispersed in a 1, 2, or 4 mol/L H_2SO_4 aqueous solution (50 mL), respectively, under stirring conditions and heated at 75 °C for 16 h. The last two acid-leaching treatments were performed in a 100 mL Teflon vessel containing a stirring bar. Once the materials were dispersed in a 4 mol/L H_2SO_4 aqueous solution (50 mL), the Teflon vessel was sealed and heated at 120 or 140 °C, respectively, under stirring conditions for 2 h with a heating rate of 5 °C/min in a microwave equipment using an irradiation power of maximum 800 W.

Synthesis of Cr@CN-800-Acid. Chitosan (0.957 g) was dispersed by sonication for 20 min in an ethanol solution of K_2CrO_4 (0.043 g in 30 mL). Afterward, the solvent was evaporated under atmospheric pressure and stirring conditions at 70 °C, and the residue was dried overnight at this temperature under high vacuum. Then, the dried sample was transferred into a quartz tube and pyrolyzed at 800 °C for 2 h in a vertical tubular oven with a ramp rate of 10 °C/min while flushing N_2 through the tube constantly until the oven was cooled down to room temperature again. The resulting material was ground in an agate mortar and transferred to a 100 mL beaker containing a stirring bar where it was dispersed in a 1 mol/L H_2SO_4 aqueous solution (50 mL) under stirring conditions and heated at 75 °C for 16 h. This material was recovered by centrifugation, washed twice with water and twice with ethanol, and dried at 60 °C.

Characterizations. Powder XRD measurements were performed in a D/MAX-2500 PC diffractometer (Rigaku) with Cu Kα radiation (l = 1.5406 Å). Samples for electron microscopy studies were prepared by sprinkling the material directly onto the holey-carbon-coated nickel or copper grids. Some of the measurements were performed in a JEM 2100F microscope operating at 200 kV both in TEM and in STEM modes. Cs-corrected STEM measurements were performed in a probe corrector Titan Themis operated at 300 kV. X-ray photoelectron spectra were acquired with a monochromatic Al Kα X-ray source (1486.6 eV) using a pass energy of 20 eV on a Kratos AXIS Ultra DLD spectrometer. The C 1s peak at 284.6 eV was used to provide a precise energy calibration. The metal content in catalysts was determined by ICP−MS using an ICP−MS Agilent 7500 CX spectrometer. Samples for ICP−MS analysis were previously digested in microwave equipment (CEM Corp., Matthews, NC) equipped with a temperature controller (MARS6 iWave). A previously weighted amount of material and 10 mL of HNO_3 (65% p/p) were introduced in a 100 mL Teflon vessel, sealed, and heated at 210 °C under static conditions for 25 min with a heating rate of 12 °C/min by irradiating at a maximum power of 1800 W. After cooling down to room temperature, the resulting solution was transferred to a previously tared 25 mL volumetric flask and diluted with Milli-Q H_2O.

^{1}H NMR spectra of isolated products were recorded on a Bruker AV 300 spectrometer. All chemical shifts (δ) are reported in parts per million (ppm) and coupling constants (J) in Hz. For ^{1}H NMR and ^{29}Si NMR, chemical shifts are reported relative to tetramethylsilane (δ 0.0 ppm in $CDCl_3$) or d-solvent peaks (δ 77.16 ppm $CDCl_3$) for ^{13}C NMR. Gas chromatography (GC) analyses were obtained on a Shimadzu GC-2010 apparatus equipped with a flame ionization detector and a Teknokroma (TBR-5MS, 30 m × 0.25 mm × 0.25 μm) column. GC−mass characterization was carried out on a GC−Mass Agilent 6890 Network equipped with a capillary column Agilent (HP-5, 30 m × 0.32 mm×0.25 μm) and a mass-selective detector. The unambiguous detection of H_2 evolved from the reaction was carried out using an Agilent 490 Micro GC equipped with two columns (Pore Plot Q and MolSieve 5A) and one thermal conductivity detector.

Raman spectra were recorded at room temperature using a 514 nm laser excitation on a Renishaw Raman spectrometer ("inVia") equipped with a charge-coupled device detector. The laser power on the sample was 10−50 mW and a total of 20 acquisitions (10 s exposure time) were taken for each spectrum. Analyses on different positions of the sample were recorded (spectral resolution ~ 2 μm). Measurements were carried out using a home-made cell, where the catalyst powder was introduced without any previous treatment.

General Procedure for the Catalytic Dehydrogenative Coupling of Silanes and Alcohols. Catalytic experiments were performed under aerobic conditions in a 50 mL round-bottom flask equipped with a reflux condenser and a magnetic stirring bar. Once the catalyst (15 mg) and the alcohol (1.5 mL) were introduced, the reaction flask was heated at 60 °C and let equilibrate for 5 min. Then, the silane (1 mmol) and anisole (54 μL, 0.5 mmol) as an internal standard were added, setting this point as the starting time of the reaction. Yields and conversions were determined by GC analysis taking samples from the reaction mixture at the reported times. No internal standard was added in reactions from which isolated yields were calculated. After reaction completion and dilution with ethyl acetate, the catalyst was separated off by filtration, and the solvent was removed under reduced pressure. Some of the products were purified by flash column chromatography using n-hexane as an eluent phase (see the Supporting Information). For the recycling experiments, the general procedure was scaled up by the factor of 7, and the reaction was performed at 30 °C in an opened 50 mL centrifugation tube. After reaction completion, the reaction mixture was diluted with ethyl acetate, and the catalyst was separated off by centrifugation, cleaned with ethyl acetate and diethyl ether, and dried at 60 °C for 30 min before using for the next run again.

■ ASSOCIATED CONTENT

Supporting Information

The Supporting Information is available free of charge at https://pubs.acs.org/doi/10.1021/acssuschemeng.0c08953.

Extended data for the characterization of catalysts, additional catalytic and Raman spectroscopic experiments, and characterization data of isolated products (PDF)

■ AUTHOR INFORMATION

Corresponding Author

Iván Sorribes − *Departament de Química Física i Analítica, Universitat Jaume I, 12071 Castellón, Spain;* orcid.org/0000-0002-3721-9335; Email: isorribe@uji.es, ivsorter@itq.upv.es

Authors

David Ventura-Espinosa − *Institute of Advanced Materials (INAM), Universitat Jaume I, 12071 Castellón, Spain*

Marcelo Assis − *Center for Development of Functional Materials (CDMF), Federal University of São Carlos, 13565-905 São Carlos, SP, Brazil;* orcid.org/0000-0003-0355-5565

Santiago Martín − *Instituto de Nanociencia y Materiales de Aragón (INMA), CSIC-Universidad de Zaragoza, 50009 Zaragoza, Spain; Departamento de Química Fisica,*

https://dx.doi.org/10.1021/acssuschemeng.0c08953
ACS Sustainable Chem. Eng. 2021, 9, 2912−2928

Universidad de Zaragoza, 50009 Zaragoza, Spain; orcid.org/0000-0001-9193-3874

Patricia Concepción − *Instituto de Tecnología Química, Universitat Politècnica de València-Consejo Superior de Investigaciones Científicas, 46022 Valencia, Spain;* orcid.org/0000-0003-2058-3103

Jefferson Bettini − *Brazilian Nanotechnology National Laboratory (LNNano), 13083-970 Campinas, Brazil*

Elson Longo − *Center for Development of Functional Materials (CDMF), Federal University of São Carlos, 13565-905 São Carlos, SP, Brazil;* orcid.org/0000-0001-8062-7791

Jose A. Mata − *Institute of Advanced Materials (INAM), Universitat Jaume I, 12071 Castellón, Spain;* orcid.org/0000-0001-9310-2783

Juan Andrés − *Departament de Química Física i Analítica, Universitat Jaume I, 12071 Castellón, Spain;* orcid.org/0000-0003-0232-3957

Complete contact information is available at: https://pubs.acs.org/10.1021/acssuschemeng.0c08953

Notes

The authors declare no competing financial interest.

■ ACKNOWLEDGMENTS

The authors thank the financial support from MICIU/AEI/FEDER (PGC2018-094417-B-I00 and RTI2018-098237-B-C22) and Universitat Jaume I (UJI-A2019-16, UJI-B2019-30, and UJI-B2018-23). I.S. thanks the Spanish Ministerio de Economía, Industria y Competitividad (MINECO) for a postdoctoral "Juan de la Cierva-Incorporación" fellowship (IJCI-2016-30590), and the financial support from the "José Castillejo" Mobility Program (CAS19/00339) of the Ministerio de Ciencia, Innovación y Universidades (MICIU). S.M. acknowledges DGA/fondos FEDER (construyendo Europa desde Aragón) for funding the research group Platón (E31_17R). D.V.-E. thanks the MICIU for a FPU grant (FPU15/03011). E.L. and M.A. thank the financial support from FAPESP (2013/07296-2), CNPq (166281/2017-4), CAPES, and FINEP. The authors also thank the "Servei Central d'Instrumentació Científica (SCIC)" of the Universitat Jaume I, as well as Dr. G. Antorrena for technical support in XPS studies.

■ REFERENCES

(1) Wuts, P. G. M.; Green, T. W. *Greene's Protective Groups in Organic Synthesis*, 4th ed.; Wiley-Interscience: New Jersey, 2006.

(2) Denmark, S. E.; Liu, J. H.-C. Silicon-Based Cross-Coupling Reactions in the Total Synthesis of Natural Products. *Angew. Chem., Int. Ed.* **2010**, *49*, 2978−2986.

(3) Crouch, R. D. Recent Advances in Silyl Protection of Alcohols. *Synth. Commun.* **2013**, *43*, 2265−2279.

(4) Schuppe, A. W.; Newhouse, T. R. Assembly of the Limonoid Architecture by a Divergent Approach: Total Synthesis of (±)-Andirolide N via (±)-8α-Hydroxycarapin. *J. Am. Chem. Soc.* **2017**, *139*, 631−634.

(5) Smith, M. B. *Organic Synthesis*, 4th ed.; Academic Press: Boston, 2017.

(6) Osterholtz, F. D.; Pohl, E. R. Kinetics of the hydrolysis and condensation of organofunctional alkoxysilanes: a review. *J. Adhes. Sci. Technol.* **1992**, *6*, 127−149.

(7) Belelli, P. G.; Ferreira, M. L.; Damiani, D. E. A theoretical and experimental study of the possible phenytriethoxysilane species found on treated silica. *J. Mol. Catal. A: Chem.* **2000**, *159*, 315−325.

(8) Díaz, I.; Pérez-Pariente, J. Synthesis of Spongelike Functionalized MCM-41 Materials from Gels Containing Amino Acids. *Chem. Mater.* **2002**, *14*, 4641−4646.

(9) Matheron, M.; Gacoin, T.; Boilot, J. P.; Bourgeois, A.; Brunet-Bruneau, A.; Rivory, J.; Jimenez, A.; Biteau, J. Ordered mesoporous organosilica films. In *Studies in Surface Science and Catalysis*; Sayari, A., Jaroniec, M., Eds.; Elsevier, 2005; Vol. *156*, pp 327−334.

(10) Shimojima, A.; Kuroda, K. Controlled synthesis of nanostructured silica-based materials from designed alkoxysilanes. *J. Sol-Gel Sci. Technol.* **2008**, *46*, 307−311.

(11) Zhou, Q.; Yan, S.; Han, C. C.; Xie, P.; Zhang, R. Promising Functional Materials Based on Ladder Polysiloxanes. *Adv. Mater.* **2008**, *20*, 2970−2976.

(12) Carrillo, A. I.; García-Martínez, J.; Llusar, R.; Serrano, E.; Sorribes, I.; Vicent, C.; Alejandro Vidal-Moya, J. Incorporation of cubane-type Mo_3S_4 molybdenum cluster sulfides in the framework of mesoporous silica. *Microporous Mesoporous Mater.* **2012**, *151*, 380−389.

(13) Kamino, B. A.; Bender, T. P. The use of siloxanes, silsesquioxanes, and silicones in organic semiconducting materials. *Chem. Soc. Rev.* **2013**, *42*, 5119−5130.

(14) Gómez-Avilés, A.; Aranda, P.; Fernandes, F. M.; Belver, C.; Ruiz-Hitzky, E. Silica-Sepiolite Nanoarchitectures. *J. Nanosci. Nanotechnol.* **2013**, *13*, 2897−2907.

(15) Negrete; Letoffe, J.-M.; Putaux, J.-L.; David, L.; Bourgeat-Lami, E. Aqueous Dispersions of Silane-Functionalized Laponite Clay Platelets. A First Step toward the Elaboration of Water-Based Polymer/Clay Nanocomposites. *Langmuir* **2004**, *20*, 1564−1571.

(16) Jaber, M.; Gaslain, F. O. M.; Miehé-Brendlé, J. Rapid and direct synthesis of spherical organotalc. *Clays Clay Miner.* **2009**, *57*, 35−39.

(17) Corey, E. J.; Venkateswarlu, A. Protection of hydroxyl groups as tert-butyldimethylsilyl derivatives. *J. Am. Chem. Soc.* **1972**, *94*, 6190−6191.

(18) Chaudhary, S. K.; Hernandez, O. 4-dimethylaminopyridine: an efficient and selective catalyst for the silylation of alcohols. *Tetrahedron Lett.* **1979**, *20*, 99−102.

(19) Kim, S.; Chang, H. 1,1,3,3-Tetramethylguanidine: An Effective Catalyst for the t-Butyldimethylsilylation of Alcohols. *Synth. Commun.* **1984**, *14*, 899−904.

(20) Patschinski, P.; Zhang, C.; Zipse, H. The Lewis Base-Catalyzed Silylation of Alcohols—A Mechanistic Analysis. *J. Org. Chem.* **2014**, *79*, 8348−8357.

(21) Melen, R. L. Dehydrocoupling routes to element−element bonds catalysed by main group compounds. *Chem. Soc. Rev.* **2016**, *45*, 775−788.

(22) Kuciński, K.; Hreczycho, G. Catalytic Formation of Silicon−Heteroatom (N, P, O, S) Bonds. *ChemCatChem* **2017**, *9*, 1868−1885.

(23) Ventura-Espinosa, D.; Carretero-Cerdán, A.; Baya, M.; García, H.; Mata, J. A. Catalytic Dehydrogenative Coupling of Hydrosilanes with Alcohols for the Production of Hydrogen On-demand: Application of a Silane/Alcohol Pair as a Liquid Organic Hydrogen Carrier. *Chem.—Eur. J.* **2017**, *23*, 10815−10821.

(24) Ventura-Espinosa, D.; Sabater, S.; Carretero-Cerdán, A.; Baya, M.; Mata, J. A. High Production of Hydrogen on Demand from Silanes Catalyzed by Iridium Complexes as a Versatile Hydrogen Storage System. *ACS Catal.* **2018**, *8*, 2558−2566.

(25) Rendler, S.; Auer, G.; Oestreich, M. Kinetic Resolution of Chiral Secondary Alcohols by Dehydrogenative Coupling with Recyclable Silicon-Stereogenic Silanes. *Angew. Chem., Int. Ed.* **2005**, *44*, 7620−7624.

(26) Corbin, R. A.; Ison, E. A.; Abu-Omar, M. M. Catalysis by cationic oxorhenium(v): hydrolysis and alcoholysis of organic silanes. *Dalton Trans.* **2009**, *15*, 2850−2855.

(27) Peterson, E.; Khalimon, A. Y.; Simionescu, R.; Kuzmina, L. G.; Howard, J. A. K.; Nikonov, G. I. Diversity of Catalysis by an Imido-Hydrido Complex of Molybdenum. Mechanism of Carbonyl Hydrosilylation and Silane Alcoholysis. *J. Am. Chem. Soc.* **2009**, *131*, 908−909.

(28) Mukherjee, D.; Thompson, R. R.; Ellern, A.; Sadow, A. D. Coordinatively Saturated Tris(oxazolinyl)borato Zinc Hydride-Catalyzed Cross Dehydrocoupling of Silanes and Alcohols. *ACS Catal.* **2011**, *1*, 698−702.
(29) Sattler, W.; Parkin, G. Zinc Catalysts for On-Demand Hydrogen Generation and Carbon Dioxide Functionalization. *J. Am. Chem. Soc.* **2012**, *134*, 17462−17465.
(30) Garcés, K.; Fernández-Alvarez, F. J.; Polo, V.; Lalrempuia, R.; Pérez-Torrente, J. J.; Oro, L. A. Iridium-Catalyzed Hydrogen Production from Hydrosilanes and Water. *ChemCatChem* **2014**, *6*, 1691−1697.
(31) Cardoso, J. M. S.; Lopes, R.; Royo, B. Dehydrogenative silylation of alcohols catalysed by half-sandwich iron N-heterocyclic carbene complexes. *J. Organomet. Chem.* **2015**, *775*, 173−177.
(32) Vijjamarri, S.; Chidara, V. K.; Rousova, J.; Du, G. Dehydrogenative coupling of alcohols and carboxylic acids with hydrosilanes catalyzed by a salen−Mn(v) complex. *Catal. Sci. Technol.* **2016**, *6*, 3886−3892.
(33) Satoh, Y.; Igarashi, M.; Sato, K.; Shimada, S. Highly Selective Synthesis of Hydrosiloxanes by Au-Catalyzed Dehydrogenative Cross-Coupling Reaction of Silanols with Hydrosilanes. *ACS Catal.* **2017**, *7*, 1836−1840.
(34) Dong, X.; Weickgenannt, A.; Oestreich, M. Broad-spectrum kinetic resolution of alcohols enabled by Cu−H-catalysed dehydrogenative coupling with hydrosilanes. *Nat. Commun.* **2017**, *8*, 15547.
(35) Vijjamarri, S.; Chidara, V. K.; Du, G. Versatile Manganese Catalysis for the Synthesis of Poly(silylether)s from Diols and Dicarbonyls with Hydrosilanes. *ACS Omega* **2017**, *2*, 582−591.
(36) Pramanik, S.; Fernandes, A.; Liautard, V.; Pucheault, M.; Robert, F.; Landais, Y. Dehydrogenative Silylation of Alcohols Under Pd-Nanoparticle Catalysis. *Chem.—Eur. J.* **2019**, *25*, 728−732.
(37) Morris, L. J.; Hill, M. S.; Mahon, M. F.; Manners, I.; McMenamy, F. S.; Whittell, G. R. Heavier Alkaline-Earth Catalyzed Dehydrocoupling of Silanes and Alcohols for the Synthesis of Metallo-Polysilylethers. *Chem.—Eur. J.* **2020**, *26*, 2954−2966.
(38) Weickgenannt, A.; Oestreich, M. Potassium tert-Butoxide-Catalyzed Dehydrogenative Si-O Coupling: Reactivity Pattern and Mechanism of an Underappreciated Alcohol Protection. *Chem.—Asian J.* **2009**, *4*, 406−410.
(39) Toutov, A. A.; Betz, K. N.; Haibach, M. C.; Romine, A. M.; Grubbs, R. H. Sodium Hydroxide Catalyzed Dehydrocoupling of Alcohols with Hydrosilanes. *Org. Lett.* **2016**, *18*, 5776−5779.
(40) Blackwell, J. M.; Foster, K. L.; Beck, V. H.; Piers, W. E. $B(C_6F_5)_3$-Catalyzed Silation of Alcohols: A Mild, General Method for Synthesis of Silyl Ethers. *J. Org. Chem.* **1999**, *64*, 4887−4892.
(41) Cella, J.; Rubinsztajn, S. Preparation of Polyaryloxysilanes and Polyaryloxysiloxanes by $B(C_6F_5)_3$ Catalyzed Polyetherification of Dihydrosilanes and Bis-Phenols. *Macromolecules* **2008**, *41*, 6965−6971.
(42) Zhou, D.; Kawakami, Y. Tris(pentafluorophenyl)borane as a Superior Catalyst in the Synthesis of Optically Active SiO-Containing Polymers. *Macromolecules* **2005**, *38*, 6902−6908.
(43) Kaźmierczak, J.; Lewandowski, D.; Hreczycho, G. $B(C_6F_5)_3$-Catalyzed Dehydrocoupling of POSS Silanols with Hydrosilanes: A Metal-Free Strategy for Effecting Functionalization of Silsesquioxanes. *Inorg. Chem.* **2020**, *59*, 9206−9214.
(44) Gao, D.; Cui, C. N-Heterocyclic Carbene Organocatalysts for Dehydrogenative Coupling of Silanes and Hydroxyl Compounds. *Chem.—Eur. J.* **2013**, *19*, 11143−11147.
(45) He, L.; Weniger, F.; Neumann, H.; Beller, M. Synthesis, Characterization, and Application of Metal Nanoparticles Supported on Nitrogen-Doped Carbon: Catalysis beyond Electrochemistry. *Angew. Chem., Int. Ed.* **2016**, *55*, 12582−12594.
(46) Cao, Y.; Mao, S.; Li, M.; Chen, Y.; Wang, Y. Metal/Porous Carbon Composites for Heterogeneous Catalysis: Old Catalysts with Improved Performance Promoted by N-Doping. *ACS Catal.* **2017**, *7*, 8090−8112.
(47) Jagadeesh, R. V.; Surkus, A.-E.; Junge, H.; Pohl, M.-M.; Radnik, J.; Rabeah, J.; Huan, H.; Schunemann, V.; Bruckner, A.; Beller, M. Nanoscale Fe_2O_3-Based Catalysts for Selective Hydrogenation of Nitroarenes to Anilines. *Science* **2013**, *342*, 1073−1076.
(48) Westerhaus, F. A.; Jagadeesh, R. V.; Wienhöfer, G.; Pohl, M.-M.; Radnik, J.; Surkus, A.-E.; Rabeah, J.; Junge, K.; Junge, H.; Nielsen, M.; Brückner, A.; Beller, M. Heterogenized cobalt oxide catalysts for nitroarene reduction by pyrolysis of molecularly defined complexes. *Nat. Chem.* **2013**, *5*, 537−543.
(49) Jagadeesh, R. V.; Junge, H.; Pohl, M.-M.; Radnik, J.; Brückner, A.; Beller, M. Selective Oxidation of Alcohols to Esters Using Heterogeneous Co_3O_4−N@C Catalysts under Mild Conditions. *J. Am. Chem. Soc.* **2013**, *135*, 10776−10782.
(50) Stemmler, T.; Surkus, A.-E.; Pohl, M.-M.; Junge, K.; Beller, M. Iron-Catalyzed Synthesis of Secondary Amines: On the Way to Green Reductive Aminations. *ChemSusChem* **2014**, *7*, 3012−3016.
(51) Stemmler, T.; Westerhaus, F. A.; Surkus, A.-E.; Pohl, M.-M.; Junge, K.; Beller, M. General and selective reductive amination of carbonyl compounds using a core−shell structured Co_3O_4/NGr@C catalyst. *Green Chem.* **2014**, *16*, 4535−4540.
(52) Jagadeesh, R. V.; Junge, H.; Beller, M. Green synthesis of nitriles using non-noble metal oxides-based nanocatalysts. *Nat. Commun.* **2014**, *5*, 4123.
(53) Jagadeesh, R. V.; Natte, K.; Junge, H.; Beller, M. Nitrogen-Doped Graphene-Activated Iron-Oxide-Based Nanocatalysts for Selective Transfer Hydrogenation of Nitroarenes. *ACS Catal.* **2015**, *5*, 1526−1529.
(54) Jagadeesh, R. V.; Stemmler, T.; Surkus, A.-E.; Bauer, M.; Pohl, M.-M.; Radnik, J.; Junge, K.; Junge, H.; Brückner, A.; Beller, M. Cobalt-based nanocatalysts for green oxidation and hydrogenation processes. *Nat. Protoc.* **2015**, *10*, 916−926.
(55) Jagadeesh, R. V.; Stemmler, T.; Surkus, A.-E.; Junge, H.; Junge, K.; Beller, M. Hydrogenation using iron oxide-based nanocatalysts for the synthesis of amines. *Nat. Protoc.* **2015**, *10*, 548−557.
(56) Jagadeesh, R. V.; Banerjee, D.; Arockiam, P. B.; Junge, H.; Junge, K.; Pohl, M.-M.; Radnik, J.; Brückner, A.; Beller, M. Highly selective transfer hydrogenation of functionalised nitroarenes using cobalt-based nanocatalysts. *Green Chem.* **2015**, *17*, 898−902.
(57) Jagadeesh, R. V.; Junge, H.; Beller, M. "Nanorust"-catalyzed Benign Oxidation of Amines for Selective Synthesis of Nitriles. *ChemSusChem* **2015**, *8*, 92−96.
(58) Westerhaus, F.; Sorribes, I.; Wienhöfer, G.; Junge, K.; Beller, M. Reduction of Nitroarenes Using CO and H_2O in the Presence of a Nanostructured Cobalt Oxide/Nitrogen-Doped Graphene (NGr) Catalyst. *Synlett* **2015**, *26*, 313−317.
(59) Chen, F.; Surkus, A.-E.; He, L.; Pohl, M.-M.; Radnik, J.; Topf, C.; Junge, K.; Beller, M. Selective Catalytic Hydrogenation of Heteroarenes with N-Graphene-Modified Cobalt Nanoparticles (Co_3O_4−Co/NGr@α-Al_2O_3). *J. Am. Chem. Soc.* **2015**, *137*, 11718−11724.
(60) Cui, X.; Li, Y.; Bachmann, S.; Scalone, M.; Surkus, A.-E.; Junge, K.; Topf, C.; Beller, M. Synthesis and Characterization of Iron−Nitrogen-Doped Graphene/Core−Shell Catalysts: Efficient Oxidative Dehydrogenation of N-Heterocycles. *J. Am. Chem. Soc.* **2015**, *137*, 10652−10658.
(61) Pisiewicz, S.; Stemmler, T.; Surkus, A.-E.; Junge, K.; Beller, M. Synthesis of Amines by Reductive Amination of Aldehydes and Ketones using Co_3O_4/NGr@C Catalyst. *ChemCatChem* **2015**, *7*, 62−64.
(62) Jagadeesh, R. V.; Stemmler, T.; Surkus, A.-E.; Bauer, M.; Pohl, M.-M.; Radnik, J.; Junge, K.; Junge, H.; Brückner, A.; Beller, M. Cobalt-based nanocatalysts for green oxidation and hydrogenation processes. *Nat. Protoc.* **2016**, *11*, 192.
(63) Natte, K.; Jagadeesh, R. V.; Sharif, M.; Neumann, H.; Beller, M. Synthesis of nitriles from amines using nanoscale Co_3O_4-based catalysts via sustainable aerobic oxidation. *Org. Biomol. Chem.* **2016**, *14*, 3356−3359.
(64) Chen, F.; Topf, C.; Radnik, J.; Kreyenschulte, C.; Lund, H.; Schneider, M.; Surkus, A.-E.; He, L.; Junge, K.; Beller, M. Stable and Inert Cobalt Catalysts for Highly Selective and Practical Hydro-

https://dx.doi.org/10.1021/acssuschemeng.0c08953
ACS Sustainable Chem. Eng. 2021, 9, 2912−2928

genation of C≡N and C=O Bonds. *J. Am. Chem. Soc.* **2016**, *138*, 8781−8788.
(65) Cui, X.; Surkus, A.-E.; Junge, K.; Topf, C.; Radnik, J.; Kreyenschulte, C.; Beller, M. Highly selective hydrogenation of arenes using nanostructured ruthenium catalysts modified with a carbon−nitrogen matrix. *Nat. Commun.* **2016**, *7*, 11326.
(66) Pisiewicz, S.; Formenti, D.; Surkus, A.-E.; Pohl, M.-M.; Radnik, J.; Junge, K.; Topf, C.; Bachmann, S.; Scalone, M.; Beller, M. Synthesis of Nickel Nanoparticles with N-Doped Graphene Shells for Catalytic Reduction Reactions. *ChemCatChem* **2016**, *8*, 129−134.
(67) Formenti, D.; Topf, C.; Junge, K.; Ragaini, F.; Beller, M. Fe_2O_3/NGr@C- and Co-Co_3O_4/NGr@C-catalysed hydrogenation of nitroarenes under mild conditions. *Catal. Sci. Technol.* **2016**, *6*, 4473−4477.
(68) Chen, F.; Sahoo, B.; Kreyenschulte, C.; Lund, H.; Zeng, M.; He, L.; Junge, K.; Beller, M. Selective cobalt nanoparticles for catalytic transfer hydrogenation of N-heteroarenes. *Chem. Sci.* **2017**, *8*, 6239−6246.
(69) Chen, F.; Kreyenschulte, C.; Radnik, J.; Lund, H.; Surkus, A.-E.; Junge, K.; Beller, M. Selective Semihydrogenation of Alkynes with N-Graphitic-Modified Cobalt Nanoparticles Supported on Silica. *ACS Catal.* **2017**, *7*, 1526−1532.
(70) Natte, K.; Neumann, H.; Jagadeesh, R. V.; Beller, M. Convenient iron-catalyzed reductive aminations without hydrogen for selective synthesis of N-methylamines. *Nat. Commun.* **2017**, *8*, 1344.
(71) Formenti, D.; Ferretti, F.; Topf, C.; Surkus, A.-E.; Pohl, M.-M.; Radnik, J.; Schneider, M.; Junge, K.; Beller, M.; Ragaini, F. Co-based heterogeneous catalysts from well-defined α-diimine complexes: Discussing the role of nitrogen. *J. Catal.* **2017**, *351*, 79−89.
(72) Chen, F.; Li, W.; Sahoo, B.; Kreyenschulte, C.; Agostini, G.; Lund, H.; Junge, K.; Beller, M. Hydrogenation of Pyridines Using a Nitrogen-Modified Titania-Supported Cobalt Catalyst. *Angew. Chem., Int. Ed.* **2018**, *57*, 14488−14492.
(73) Sahoo, B.; Kreyenschulte, C.; Agostini, G.; Lund, H.; Bachmann, S.; Scalone, M.; Junge, K.; Beller, M. A robust iron catalyst for the selective hydrogenation of substituted (iso)-quinolones. *Chem. Sci.* **2018**, *9*, 8134−8141.
(74) Ryabchuk, P.; Agostini, G.; Pohl, M.-M.; Lund, H.; Agapova, A.; Junge, H.; Junge, K.; Beller, M. Intermetallic nickel silicide nanocatalyst—A non-noble metal-based general hydrogenation catalyst. *Sci. Adv.* **2018**, *4*, No. eaat0761.
(75) Fiorio, J. L.; Gonçalves, R. V.; Teixeira-Neto, E.; Ortuño, M. A.; López, N.; Rossi, L. M. Accessing Frustrated Lewis Pair Chemistry through Robust Gold@N-Doped Carbon for Selective Hydrogenation of Alkynes. *ACS Catal.* **2018**, *8*, 3516−3524.
(76) Li, G.; Yang, H.; Zhang, H.; Qi, Z.; Chen, M.; Hu, W.; Tian, L.; Nie, R.; Huang, W. Encapsulation of Nonprecious Metal into Ordered Mesoporous N-Doped Carbon for Efficient Quinoline Transfer Hydrogenation with Formic Acid. *ACS Catal.* **2018**, *8*, 8396−8405.
(77) Li, W.; Artz, J.; Broicher, C.; Junge, K.; Hartmann, H.; Besmehn, A.; Palkovits, R.; Beller, M. Superior activity and selectivity of heterogenized cobalt catalysts for hydrogenation of nitroarenes. *Catal. Sci. Technol.* **2019**, *9*, 157−162.
(78) Ryabchuk, P.; Agapova, A.; Kreyenschulte, C.; Lund, H.; Junge, H.; Junge, K.; Beller, M. Heterogeneous nickel-catalysed reversible, acceptorless dehydrogenation of N-heterocycles for hydrogen storage. *Chem. Commun.* **2019**, *55*, 4969−4972.
(79) Lange, S.; Formenti, D.; Lund, H.; Kreyenschulte, C.; Agostini, G.; Bartling, S.; Bachmann, S.; Scalone, M.; Junge, K.; Beller, M. Additive-Free Nickel-Catalyzed Debenzylation Reactions via Hydrogenative C−O and C−N Bond Cleavage. *ACS Sustainable Chem. Eng.* **2019**, *7*, 17107−17113.
(80) Wu, Y.; Wang, T.; Wang, H.; Wang, X.; Dai, X.; Shi, F. Active catalyst construction for CO_2 recycling via catalytic synthesis of N-doped carbon on supported Cu. *Nat. Commun.* **2019**, *10*, 2599.
(81) Xu, L.; Nie, R.; Lyu, X.; Wang, J.; Lu, X. Selective hydrogenation of furfural to furfuryl alcohol without external hydrogen over N-doped carbon confined Co catalysts. *Fuel Process. Technol.* **2020**, *197*, 106205.
(82) Zhong, W.; Liu, H.; Bai, C.; Liao, S.; Li, Y. Base-Free Oxidation of Alcohols to Esters at Room Temperature and Atmospheric Conditions using Nanoscale Co-Based Catalysts. *ACS Catal.* **2015**, *5*, 1850−1856.
(83) Zhou, Y.-X.; Chen, Y.-Z.; Cao, L.; Lu, J.; Jiang, H.-L. Conversion of a metal−organic framework to N-doped porous carbon incorporating Co and CoO nanoparticles: direct oxidation of alcohols to esters. *Chem. Commun.* **2015**, *51*, 8292−8295.
(84) Shen, K.; Chen, X.; Chen, J.; Li, Y. Development of MOF-Derived Carbon-Based Nanomaterials for Efficient Catalysis. *ACS Catal.* **2016**, *6*, 5887−5903.
(85) Bai, C.; Li, A.; Yao, X.; Liu, H.; Li, Y. Efficient and selective aerobic oxidation of alcohols catalysed by MOF-derived Co catalysts. *Green Chem.* **2016**, *18*, 1061−1069.
(86) Jagadeesh, R. V.; Murugesan, K.; Alshammari, A. S.; Neumann, H.; Pohl, M.-M.; Radnik, J.; Beller, M. MOF-derived cobalt nanoparticles catalyze a general synthesis of amines. *Science* **2017**, *358*, 326.
(87) Dang, S.; Zhu, Q.-L.; Xu, Q. Nanomaterials derived from metal−organic frameworks. *Nat. Rev. Mater.* **2017**, *3*, 17075.
(88) Fang, R.; Tian, P.; Yang, X.; Luque, R.; Li, Y. Encapsulation of ultrafine metal-oxide nanoparticles within mesopores for biomass-derived catalytic applications. *Chem. Sci.* **2018**, *9*, 1854−1859.
(89) Wang, Q.; Tsumori, N.; Kitta, M.; Xu, Q. Fast Dehydrogenation of Formic Acid over Palladium Nanoparticles Immobilized in Nitrogen-Doped Hierarchically Porous Carbon. *ACS Catal.* **2018**, *8*, 12041−12045.
(90) Zhang, W.; Wu, W.; Long, Y.; Wang, F.; Ma, J. Co-Ag alloy protected by nitrogen doped carbon as highly efficient and chemoselective catalysts for the hydrogenation of halogenated nitrobenzenes. *J. Colloid Interface Sci.* **2018**, *522*, 217−227.
(91) Bennedsen, N. R.; Kramer, S.; Mielby, J. J.; Kegnæs, S. Cobalt−nickel alloy catalysts for hydrosilylation of ketones synthesized by utilizing metal−organic framework as template. *Catal. Sci. Technol.* **2018**, *8*, 2434−2440.
(92) Bhadra, B. N.; Vinu, A.; Serre, C.; Jhung, S. H. MOF-derived carbonaceous materials enriched with nitrogen: Preparation and applications in adsorption and catalysis. *Mater. Today* **2019**, *25*, 88−111.
(93) Lee, K. J.; Lee, J. H.; Jeoung, S.; Moon, H. R. Transformation of Metal−Organic Frameworks/Coordination Polymers into Functional Nanostructured Materials: Experimental Approaches Based on Mechanistic Insights. *Acc. Chem. Res.* **2017**, *50*, 2684−2692.
(94) Nandi, S.; Saha, A.; Patel, P.; Khan, N.-u. H.; Kureshy, R. I.; Panda, A. B. Hydrogenation of Furfural with Nickel Nanoparticles Stabilized on Nitrogen-Rich Carbon Core−Shell and Its Transformations for the Synthesis of γ-Valerolactone in Aqueous Conditions. *ACS Appl. Mater. Interfaces* **2018**, *10*, 24480−24490.
(95) Murugesan, K.; Senthamarai, T.; Alshammari, A. S.; Altamimi, R. M.; Kreyenschulte, C.; Pohl, M.-M.; Lund, H.; Jagadeesh, R. V.; Beller, M. Cobalt-Nanoparticles Catalyzed Efficient and Selective Hydrogenation of Aromatic Hydrocarbons. *ACS Catal.* **2019**, *9*, 8581−8591.
(96) Mondal, D.; Sharma, M.; Wang, C.-H.; Lin, Y.-C.; Huang, H.-C.; Saha, A.; Nataraj, S. K.; Prasad, K. Deep eutectic solvent promoted one step sustainable conversion of fresh seaweed biomass to functionalized graphene as a potential electrocatalyst. *Green Chem.* **2016**, *18*, 2819−2826.
(97) Yao, W.-T.; Yu, L.; Yao, P.-F.; Wei, K.; Han, S.-L.; Chen, P.; Xie, J.-S. Bulk Production of Nonprecious Metal Catalysts from Cheap Starch as Precursor and Their Excellent Electrochemical Activity. *ACS Sustainable Chem. Eng.* **2016**, *4*, 3235−3244.
(98) Ji, G.; Duan, Y.; Zhang, S.; Fei, B.; Chen, X.; Yang, Y. Selective Semihydrogenation of Alkynes Catalyzed by Pd Nanoparticles Immobilized on Heteroatom-Doped Hierarchical Porous Carbon Derived from Bamboo Shoots. *ChemSusChem* **2017**, *10*, 3427−3434.

https://dx.doi.org/10.1021/acssuschemeng.0c08953
ACS Sustainable Chem. Eng. 2021, 9, 2912−2928

(99) Yang, H.; Nie, R.; Xia, W.; Yu, X.; Jin, D.; Lu, X.; Zhou, D.; Xia, Q. Co embedded within biomass-derived mesoporous N-doped carbon as an acid-resistant and chemoselective catalyst for transfer hydrodeoxygenation of biomass with formic acid. *Green Chem.* **2017**, *19*, 5714−5722.
(100) Duan, Y.; Ji, G.; Zhang, S.; Chen, X.; Yang, Y. Additive-modulated switchable reaction pathway in the addition of alkynes with organosilanes catalyzed by supported Pd nanoparticles: hydrosilylation versus semihydrogenation. *Catal. Sci. Technol.* **2018**, *8*, 1039−1050.
(101) Duan, Y.; Song, T.; Dong, X.; Yang, Y. Enhanced catalytic performance of cobalt nanoparticles coated with a N,P-codoped carbon shell derived from biomass for transfer hydrogenation of functionalized nitroarenes. *Green Chem.* **2018**, *20*, 2821−2828.
(102) Song, T.; Ren, P.; Duan, Y.; Wang, Z.; Chen, X.; Yang, Y. Cobalt nanocomposites on N-doped hierarchical porous carbon for highly selective formation of anilines and imines from nitroarenes. *Green Chem.* **2018**, *20*, 4629−4637.
(103) Ma, Z.; Song, T.; Yuan, Y.; Yang, Y. Synergistic catalysis on Fe−Nx sites and Fe nanoparticles for efficient synthesis of quinolines and quinazolinones via oxidative coupling of amines and aldehydes. *Chem. Sci.* **2019**, *10*, 10283−10289.
(104) Zhou, S.; Dai, F.; Dang, C.; Wang, M.; Liu, D.; Lu, F.; Qi, H. Scale-up biopolymer-chelated fabrication of cobalt nanoparticles encapsulated in N-enriched graphene shells for biofuel upgrade with formic acid. *Green Chem.* **2019**, *21*, 4732−4747.
(105) Zhang, W.; Oulego, P.; Slot, T. K.; Rothenberg, G.; Shiju, N. R. Selective Aerobic Oxidation of Lactate to Pyruvate Catalyzed by Vanadium-Nitrogen-Doped Carbon Nanosheets. *ChemCatChem* **2019**, *11*, 3381−3387.
(106) Chen, X.; Yang, H.; Yan, N. Shell Biorefinery: Dream or Reality? *Chem.—Eur. J.* **2016**, *22*, 13402−13421.
(107) Zhao, L.; Baccile, N.; Gross, S.; Zhang, Y.; Wei, W.; Sun, Y.; Antonietti, M.; Titirici, M.-M. Sustainable nitrogen-doped carbonaceous materials from biomass derivatives. *Carbon* **2010**, *48*, 3778−3787.
(108) Primo, A.; Atienzar, P.; Sanchez, E.; Delgado, J. M.; García, H. From biomass wastes to large-area, high-quality, N-doped graphene: catalyst-free carbonization of chitosan coatings on arbitrary substrates. *Chem. Commun.* **2012**, *48*, 9254−9256.
(109) Dhakshinamoorthy, A.; Primo, A.; Concepcion, P.; Alvaro, M.; Garcia, H. Doped Graphene as a Metal-Free Carbocatalyst for the Selective Aerobic Oxidation of Benzylic Hydrocarbons, Cyclooctane and Styrene. *Chem.—Eur. J.* **2013**, *19*, 7547−7554.
(110) Primo, A.; Neatu, F.; Florea, M.; Parvulescu, V.; Garcia, H. Graphenes in the absence of metals as carbocatalysts for selective acetylene hydrogenation and alkene hydrogenation. *Nat. Commun.* **2014**, *5*, 5291.
(111) Liu, Q.; Duan, Y.; Zhao, Q.; Pan, F.; Zhang, B.; Zhang, J. Direct Synthesis of Nitrogen-Doped Carbon Nanosheets with High Surface Area and Excellent Oxygen Reduction Performance. *Langmuir* **2014**, *30*, 8238−8245.
(112) Lavorato, C.; Primo, A.; Molinari, R.; Garcia, H. N-Doped Graphene Derived from Biomass as a Visible-Light Photocatalyst for Hydrogen Generation from Water/Methanol Mixtures. *Chem.—Eur. J.* **2014**, *20*, 187−194.
(113) Hao, P.; Zhao, Z.; Leng, Y.; Tian, J.; Sang, Y.; Boughton, R. I.; Wong, C. P.; Liu, H.; Yang, B. Graphene-based nitrogen self-doped hierarchical porous carbon aerogels derived from chitosan for high performance supercapacitors. *Nano Energy* **2015**, *15*, 9−23.
(114) Wang, Y.-Y.; Hou, B.-H.; Lü, H.-Y.; Wan, F.; Wang, J.; Wu, X.-L. Porous N-doped carbon material derived from prolific chitosan biomass as a high-performance electrode for energy storage. *RSC Adv.* **2015**, *5*, 97427−97434.
(115) Wu, T. X.; Wang, G. Z.; Zhang, X.; Chen, C.; Zhang, Y. X.; Zhao, H. J. Transforming chitosan into N-doped graphitic carbon electrocatalysts. *Chem. Commun.* **2015**, *51*, 1334−1337.
(116) Deng, J.; Li, M.; Wang, Y. Biomass-derived carbon: synthesis and applications in energy storage and conversion. *Green Chem.* **2016**, *18*, 4824−4854.
(117) Zhao, J.; Liu, Y.; Quan, X.; Chen, S.; Yu, H.; Zhao, H. Nitrogen-doped carbon with a high degree of graphitization derived from biomass as high-performance electrocatalyst for oxygen reduction reaction. *Appl. Surf. Sci.* **2017**, *396*, 986−993.
(118) Raghavan, N.; Thangavel, S.; Venugopal, G. A short review on preparation of graphene from waste and bioprecursors. *Appl. Mater. Today* **2017**, *7*, 246−254.
(119) Rizescu, C.; Podolean, I.; Albero, J.; Parvulescu, V. I.; Coman, S. M.; Bucur, C.; Puche, M.; Garcia, H. N-Doped graphene as a metal-free catalyst for glucose oxidation to succinic acid. *Green Chem.* **2017**, *19*, 1999−2005.
(120) Garcia, A.; Albero, J.; García, H. Multilayer N-doped Graphene Films as Photoelectrodes for H_2 Evolution. *ChemPhotoChem* **2017**, *1*, 388−392.
(121) Esteve-Adell, I.; He, J.; Ramiro, F.; Atienzar, P.; Primo, A.; García, H. Catalyst-free one step synthesis of large area vertically stacked N-doped graphene-boron nitride heterostructures from biomass source. *Nanoscale* **2018**, *10*, 4391−4397.
(122) He, J.; Anouar, A.; Primo, A.; García, H. Quality Improvement of Few-Layers Defective Graphene from Biomass and Application for H2 Generation. *Nanomaterials* **2019**, *9*, 895.
(123) Varma, A. J.; Deshpande, S. V.; Kennedy, J. F. Metal complexation by chitosan and its derivatives: a review. *Carbohydr. Polym.* **2004**, *55*, 77−93.
(124) Guibal, E. Interactions of metal ions with chitosan-based sorbents: a review. *Sep. Purif. Technol.* **2004**, *38*, 43−74.
(125) Wang, X.; Du, Y.; Fan, L.; Liu, H.; Hu, Y. Chitosan−metal complexes as antimicrobial agent: Synthesis, characterization and Structure-activity study. *Polym. Bull.* **2005**, *55*, 105−113.
(126) Guibal, E. Heterogeneous catalysis on chitosan-based materials: a review. *Prog. Polym. Sci.* **2005**, *30*, 71−109.
(127) Taboada, E.; Cabrera, G.; Jimenez, R.; Cardenas, G. A kinetic study of the thermal degradation of chitosan-metal complexes. *J. Appl. Polym. Sci.* **2009**, *114*, 2043−2052.
(128) Yan, N.; Chen, X. Sustainability: Don't waste seafood waste. *Nature* **2015**, *524*, 155−157.
(129) Blandez, J. F.; Primo, A.; Asiri, A. M.; Álvaro, M.; García, H. Copper Nanoparticles Supported on Doped Graphenes as Catalyst for the Dehydrogenative Coupling of Silanes and Alcohols. *Angew. Chem., Int. Ed.* **2014**, *53*, 12581−12586.
(130) Primo, A.; Esteve-Adell, I.; Blandez, J. F.; Dhakshinamoorthy, A.; Álvaro, M.; Candu, N.; Coman, S. M.; Parvulescu, V. I.; García, H. High catalytic activity of oriented 2.0.0 copper(I) oxide grown on graphene film. *Nat. Commun.* **2015**, *6*, 8561.
(131) Hurtado, L.; Natividad, R.; García, H. Photocatalytic activity of Cu_2O supported on multi layers graphene for CO_2 reduction by water under batch and continuous flow. *Catal. Commun.* **2016**, *84*, 30−35.
(132) Mateo, D.; Esteve-Adell, I.; Albero, J.; Primo, A.; García, H. Oriented 2.0.0 Cu_2O nanoplatelets supported on few-layers graphene as efficient visible light photocatalyst for overall water splitting. *Appl. Catal., B* **2017**, *201*, 582−590.
(133) Primo, A.; Esteve-Adell, I.; Coman, S. N.; Candu, N.; Parvulescu, V. I.; Garcia, H. One-Step Pyrolysis Preparation of 1.1.1 Oriented Gold Nanoplatelets Supported on Graphene and Six Orders of Magnitude Enhancement of the Resulting Catalytic Activity. *Angew. Chem., Int. Ed.* **2016**, *55*, 607−612.
(134) Esteve-Adell, I.; Bakker, N.; Primo, A.; Hensen, E.; García, H. Oriented Pt Nanoparticles Supported on Few-Layers Graphene as Highly Active Catalyst for Aqueous-Phase Reforming of Ethylene Glycol. *ACS Appl. Mater. Interfaces* **2016**, *8*, 33690−33696.
(135) Dhakshinamoorthy, A.; Esteve Adell, I.; Primo, A.; Garcia, H. Enhanced Activity of Ag Nanoplatelets on Few Layers of Graphene Film with Preferential Orientation for Dehydrogenative Silane−Alcohol Coupling. *ACS Sustainable Chem. Eng.* **2017**, *5*, 2400−2406.

https://dx.doi.org/10.1021/acssuschemeng.0c08953
ACS Sustainable Chem. Eng. 2021, 9, 2912−2928

(136) Sahoo, B.; Surkus, A.-E.; Pohl, M.-M.; Radnik, J.; Schneider, M.; Bachmann, S.; Scalone, M.; Junge, K.; Beller, M. A Biomass-Derived Non-Noble Cobalt Catalyst for Selective Hydrodehalogenation of Alkyl and (Hetero)Aryl Halides. *Angew. Chem., Int. Ed.* **2017**, *56*, 11242−11247.
(137) Sahoo, B.; Formenti, D.; Topf, C.; Bachmann, S.; Scalone, M.; Junge, K.; Beller, M. Biomass-Derived Catalysts for Selective Hydrogenation of Nitroarenes. *ChemSusChem* **2017**, *10*, 3035−3039.
(138) Scharnagl, F. K.; Hertrich, M. F.; Ferretti, F.; Kreyenschulte, C.; Lund, H.; Jackstell, R.; Beller, M. Hydrogenation of terminal and internal olefins using a biowaste-derived heterogeneous cobalt catalyst. *Sci. Adv.* **2018**, *4*, No. eaau1248.
(139) Hertrich, M. F.; Scharnagl, F. K.; Pews-Davtyan, A.; Kreyenschulte, C. R.; Lund, H.; Bartling, S.; Jackstell, R.; Beller, M. Supported Cobalt Nanoparticles for Hydroformylation Reactions. *Chem.—Eur. J.* **2019**, *25*, 5534−5538.
(140) Lee, D.-W.; Jin, M.-H.; Oh, D.; Lee, S.-W.; Park, J.-S. Straightforward Synthesis of Hierarchically Porous Nitrogen-Doped Carbon via Pyrolysis of Chitosan/Urea/KOH Mixtures and Its Application as a Support for Formic Acid Dehydrogenation Catalysts. *ACS Sustainable Chem. Eng.* **2017**, *5*, 9935−9944.
(141) He, J.; Dhakshinamoorthy, A.; Primo, A.; Garcia, H. Iron Nanoparticles Embedded in Graphitic Carbon Matrix as Heterogeneous Catalysts for the Oxidative C−N Coupling of Aromatic N−H Compounds and Amides. *ChemCatChem* **2017**, *9*, 3003−3012.
(142) Zhang, F.; Ma, C.; Chen, S.; Zhang, J.; Li, Z.; Zhang, X.-M. N-doped hierarchical porous carbon anchored tiny Pd NPs: A mild and efficient quinolines selective hydrogenation catalyst. *Mol. Catal.* **2018**, *452*, 145−153.
(143) Bi, Q.-Y.; Lin, J.-D.; Liu, Y.-M.; He, H.-Y.; Huang, F.-Q.; Cao, Y. Dehydrogenation of Formic Acid at Room Temperature: Boosting Palladium Nanoparticle Efficiency by Coupling with Pyridinic-Nitrogen-Doped Carbon. *Angew. Chem., Int. Ed.* **2016**, *55*, 11849−11853.
(144) Chen, B.; Zhang, C.; Niu, L.; Shi, X.; Zhang, H.; Lan, X.; Bai, G. Biomass-Derived N-doped Carbon Materials with Silica-Supported Ultrasmall ZnO Nanoparticles: Robust Catalysts for the Green Synthesis of Benzimidazoles. *Chem.—Eur. J.* **2018**, *24*, 3481−3487.
(145) Xu, M.; Zhao, J.; Shu, G.; Zheng, X.; Liu, Q.; Wang, Y.; Zeng, M. One-pot carbonization of chitosan/P123/PdCl2 blend hydrogel membranes to N-doped carbon supported Pd catalytic composites for Ullmann reactions. *Int. J. Biol. Macromol.* **2019**, *125*, 213−220.
(146) Vasilev, A. A.; Efimov, M. N.; Bondarenko, G. N.; Muratov, D. G.; Dzidziguri, E. L.; Ivantsov, M. I.; Kulikova, M. V.; Karpacheva, G. P. FeCo alloy nanoparticles supported on IR pyrolyzed chitosan as catalyst for Fischer−Tropsch synthesis. *Chem. Phys. Lett.* **2019**, *730*, 8−13.
(147) Thombal, P. R.; Thombal, R. S.; Han, S. S. Chitosan-derived N-doped carbon catalysts with a metallic core for the oxidative dehydrogenation of NH−NH bonds. *RSC Adv.* **2020**, *10*, 474−481.
(148) Liang, B.; Zhao, Y.; Li, K.; Lv, C. Porous carbon codoped with inherent nitrogen and externally embedded cobalt nanoparticles as a high-performance cathode catalyst for microbial fuel cells. *Appl. Surf. Sci.* **2020**, *505*, 144547.
(149) Lin, Y.; Lu, G.-P.; Zhao, X.; Cao, X.; Yang, L.; Zhou, B.; Zhong, Q.; Chen, Z. Porous cobalt@N-doped carbon derived from chitosan for oxidative esterification of 5-Hydroxymethylfurfural: The roles of zinc in the synthetic and catalytic process. *Mol. Catal.* **2020**, *482*, 110695.
(150) Zhang, L.; Wang, A.; Wang, W.; Huang, Y.; Liu, X.; Miao, S.; Liu, J.; Zhang, T. Co−N−C Catalyst for C−C Coupling Reactions: On the Catalytic Performance and Active Sites. *ACS Catal.* **2015**, *5*, 6563−6572.
(151) Liu, W.; Zhang, L.; Yan, W.; Liu, X.; Yang, X.; Miao, S.; Wang, W.; Wang, A.; Zhang, T. Single-atom dispersed Co−N−C catalyst: structure identification and performance for hydrogenative coupling of nitroarenes. *Chem. Sci.* **2016**, *7*, 5758−5764.
(152) Tang, C.; Surkus, A.-E.; Chen, F.; Pohl, M.-M.; Agostini, G.; Schneider, M.; Junge, H.; Beller, M. A Stable Nanocobalt Catalyst with Highly Dispersed CoNx Active Sites for the Selective Dehydrogenation of Formic Acid. *Angew. Chem., Int. Ed.* **2017**, *56*, 16616−16620.
(153) Liu, W.; Zhang, L.; Liu, X.; Liu, X.; Yang, X.; Miao, S.; Wang, W.; Wang, A.; Zhang, T. Discriminating Catalytically Active FeNx Species of Atomically Dispersed Fe−N−C Catalyst for Selective Oxidation of the C−H Bond. *J. Am. Chem. Soc.* **2017**, *139*, 10790−10798.
(154) Chen, Y.; Huang, Z.; Ma, Z.; Chen, J.; Tang, X. Fabrication, characterization, and stability of supported single-atom catalysts. *Catal. Sci. Technol.* **2017**, *7*, 4250−4258.
(155) Lai, W. H.; Miao, Z.; Wang, Y. X.; Wang, J. Z.; Chou, S. L. Atomic-Local Environments of Single-Atom Catalysts: Synthesis, Electronic Structure, and Activity. *Adv. Energy Mater.* **2019**, *9*, 1900722.
(156) Qiu, J.-Z.; Hu, J.; Lan, J.; Wang, L.-F.; Fu, G.; Xiao, R.; Ge, B.; Jiang, J. Pure Siliceous Zeolite-Supported Ru Single-Atom Active Sites for Ammonia Synthesis. *Chem. Mater.* **2019**, *31*, 9413−9421.
(157) Gawande, M. B.; Fornasiero, P.; Zbořil, R. Carbon-Based Single-Atom Catalysts for Advanced Applications. *ACS Catal.* **2020**, *10*, 2231−2259.
(158) Li, Z.; Ji, S.; Liu, Y.; Cao, X.; Tian, S.; Chen, Y.; Niu, Z.; Li, Y. Well-Defined Materials for Heterogeneous Catalysis: From Nanoparticles to Isolated Single-Atom Sites. *Chem. Rev.* **2020**, *120*, 623−682.
(159) Chen, W.; Pei, J.; He, C.-T.; Wan, J.; Ren, H.; Zhu, Y.; Wang, Y.; Dong, J.; Tian, S.; Cheong, W.-C.; Lu, S.; Zheng, L.; Zheng, X.; Yan, W.; Zhuang, Z.; Chen, C.; Peng, Q.; Wang, D.; Li, Y. Rational Design of Single Molybdenum Atoms Anchored on N-Doped Carbon for Effective Hydrogen Evolution Reaction. *Angew. Chem., Int. Ed.* **2017**, *56*, 16086−16090.
(160) Zhu, Y.; Sun, W.; Chen, W.; Cao, T.; Xiong, Y.; Luo, J.; Dong, J.; Zheng, L.; Zhang, J.; Wang, X.; Chen, C.; Peng, Q.; Wang, D.; Li, Y. Scale-Up Biomass Pathway to Cobalt Single-Site Catalysts Anchored on N-Doped Porous Carbon Nanobelt with Ultrahigh Surface Area. *Adv. Funct. Mater.* **2018**, *28*, 1802167.
(161) Sommer, L. H.; Lyons, J. E. Stereochemistry of asymmetric silicon. XVI. Transition metal catalyzed substitution reactions of optically active organosilicon hydrides. *J. Am. Chem. Soc.* **1969**, *91*, 7061−7067.
(162) Yamamoto, K.; Takemae, M. The Utility of t-Butyldimethylsilane as an Effective Silylation Reagent for the Protection of Functional Groups. *Bull. Chem. Soc. Jpn.* **1989**, *62*, 2111−2113.
(163) Chung, M.-K.; Orlova, G.; Goddard, J. D.; Schlaf, M.; Harris, R.; Beveridge, T. J.; White, G.; Hallett, F. R. Regioselective Silylation of Sugars through Palladium Nanoparticle-Catalyzed Silane Alcoholysis. *J. Am. Chem. Soc.* **2002**, *124*, 10508−10518.
(164) Raffa, P.; Evangelisti, C.; Vitulli, G.; Salvadori, P. First examples of gold nanoparticles catalyzed silane alcoholysis and silylative pinacol coupling of carbonyl compounds. *Tetrahedron Lett.* **2008**, *49*, 3221−3224.
(165) Kim, S.; Kwon, M. S.; Park, J. Silylation of primary alcohols with recyclable ruthenium catalyst and hydrosilanes. *Tetrahedron Lett.* **2010**, *51*, 4573−4575.
(166) Taguchi, T.; Isozaki, K.; Miki, K. Enhanced Catalytic Activity of Self-Assembled-Monolayer-Capped Gold Nanoparticles. *Adv. Mater.* **2012**, *24*, 6462−6467.
(167) Mitschang, F.; Schmalz, H.; Agarwal, S.; Greiner, A. Tea-Bag-Like Polymer Nanoreactors Filled with Gold Nanoparticles. *Angew. Chem., Int. Ed.* **2014**, *53*, 4972−4975.
(168) Li, Z.; Lin, S.; Ji, L.; Zhang, Z.; Zhang, X.; Ding, Y. Nanoporous palladium catalyzed silicon-based one-pot cross-coupling reaction of aryl iodides with organosilanes. *Catal. Sci. Technol.* **2014**, *4*, 1734−1737.
(169) Li, Z.; Xu, X.; Zhang, X. Oxidation of Organosilanes with Nanoporous Copper as a Sustainable Non-Noble-Metal Catalyst. *ChemPhysChem* **2015**, *16*, 1603−1606.

https://dx.doi.org/10.1021/acssuschemeng.0c08953
ACS Sustainable Chem. Eng. 2021, 9, 2912−2928

(170) Dhakshinamoorthy, A.; Concepcion, P.; Garcia, H. Dehydrogenative coupling of silanes with alcohols catalyzed by $Cu_3(BTC)_2$. *Chem. Commun.* **2016**, *52*, 2725−2728.
(171) Wang, C.; Lin, X.; Ge, Y.; Shah, Z. H.; Lu, R.; Zhang, S. Silica-supported ultra small gold nanoparticles as nanoreactors for the etherification of silanes. *RSC Adv.* **2016**, *6*, 102102−102108.
(172) Wang, C.; Zhang, Z.; Yang, G.; Chen, Q.; Yin, Y.; Jin, M. Creation of Controllable High-Density Defects in Silver Nanowires for Enhanced Catalytic Property. *Nano Lett.* **2016**, *16*, 5669−5674.
(173) Schöbel, J.; Burgard, M.; Hils, C.; Dersch, R.; Dulle, M.; Volk, K.; Karg, M.; Greiner, A.; Schmalz, H. Bottom-Up Meets Top-Down: Patchy Hybrid Nonwovens as an Efficient Catalysis Platform. *Angew. Chem., Int. Ed.* **2017**, *56*, 405−408.
(174) Lin, J.-D.; Bi, Q.-Y.; Tao, L.; Jiang, T.; Liu, Y.-M.; He, H.-Y.; Cao, Y.; Wang, Y.-D. Wettability-Driven Palladium Catalysis for Enhanced Dehydrogenative Coupling of Organosilanes. *ACS Catal.* **2017**, *7*, 1720−1727.
(175) Anbu, N.; Dhakshinamoorthy, A. $Cu_3(BTC)_2$ catalyzed dehydrogenative coupling of dimethylphenylsilane with phenol and homocoupling of dimethylphenylsilane to disiloxane. *J. Colloid Interface Sci.* **2017**, *490*, 430−435.
(176) Dhiman, M.; Chalke, B.; Polshettiwar, V. Organosilane oxidation with a half million turnover number using fibrous nanosilica supported ultrasmall nanoparticles and pseudo-single atoms of gold. *J. Mater. Chem. A* **2017**, *5*, 1935−1940.
(177) Dai, Y.; Xing, P.; Cui, X.; Li, Z.; Zhang, X. Coexistence of Cu(ii) and Cu(i) in Cu ion-doped zeolitic imidazolate frameworks (ZIF-8) for the dehydrogenative coupling of silanes with alcohols. *Dalton Trans.* **2019**, *48*, 16562−16568.
(178) Wang, C.; Li, X.; Jin, L.; Lu, P.-H.; Dejoie, C.; Zhu, W.; Wang, Z.; Bi, W.; Dunin-Borkowski, R. E.; Chen, K.; Jin, M. Etching-Assisted Route to Heterophase Au Nanowires with Multiple Types of Active Surface Sites for Silane Oxidation. *Nano Lett.* **2019**, *19*, 6363−6369.
(179) Li, H.; Guo, H.; Li, Z.; Wu, C.; Li, J.; Zhao, C.; Guo, S.; Ding, Y.; He, W.; Li, Y. Silylation reactions on nanoporous gold via homolytic Si−H activation of silanes. *Chem. Sci.* **2018**, *9*, 4808−4813.
(180) Wang, X.; Li, P.; Li, Z.; Chen, W.; Zhou, H.; Zhao, Y.; Wang, X.; Zheng, L.; Dong, J.; Lin, Y.; Zheng, X.; Yan, W.; Yang, J.; Yang, Z.; Qu, Y.; Yuan, T.; Wu, Y.; Li, Y. 2D MOF induced accessible and exclusive Co single sites for an efficient O-silylation of alcohols with silanes. *Chem. Commun.* **2019**, *55*, 6563−6566.
(181) Chen, B.; Li, F.; Mei, Q.; Yang, Y.; Liu, H.; Yuan, G.; Han, B. Synthesis of nitrogen and sulfur co-doped hierarchical porous carbons and metal-free oxidative coupling of silanes with alcohols. *Chem. Commun.* **2017**, *53*, 13019−13022.
(182) Mitsudome, T.; Arita, S.; Mori, H.; Mizugaki, T.; Jitsukawa, K.; Kaneda, K. Supported Silver-Nanoparticle-Catalyzed Highly Efficient Aqueous Oxidation of Phenylsilanes to Silanols. *Angew. Chem., Int. Ed.* **2008**, *47*, 7938−7940.
(183) Kikukawa, Y.; Kuroda, Y.; Yamaguchi, K.; Mizuno, N. Diamond-Shaped $[Ag_4]^{4+}$ Cluster Encapsulated by Silicotungstate Ligands: Synthesis and Catalysis of Hydrolytic Oxidation of Silanes. *Angew. Chem., Int. Ed.* **2012**, *51*, 2434−2437.
(184) Li, Z.; Zhang, C.; Tian, J.; Zhang, Z.; Zhang, X.; Ding, Y. Highly selective oxidation of organosilanes with a reusable nanoporous silver catalyst. *Catal. Commun.* **2014**, *53*, 53−56.
(185) Teo, A. K. L.; Fan, W. Y. Catalytic hydrogen evolution from hydrolytic oxidation of organosilanes with silver nitrate catalyst. *RSC Adv.* **2014**, *4*, 37645−37648.
(186) Fan, L.; Liu, P. F.; Yan, X.; Gu, L.; Yang, Z. Z.; Yang, H. G.; Qiu, S.; Yao, X. Atomically isolated nickel species anchored on graphitized carbon for efficient hydrogen evolution electrocatalysis. *Nat. Commun.* **2016**, *7*, 10667.
(187) Zhang, H.; Wang, G.; Chen, D.; Lv, X.; Li, J. Tuning Photoelectrochemical Performances of Ag−TiO_2 Nanocomposites via Reduction/Oxidation of Ag. *Chem. Mater.* **2008**, *20*, 6543−6549.
(188) Liu, Y.; Fang, L.; Lu, H.; Li, Y.; Hu, C.; Yu, H. One-pot pyridine-assisted synthesis of visible-light-driven photocatalyst Ag/Ag_3PO_4. *Appl. Catal., B* **2012**, *115*−*116*, 245−252.
(189) Zhang, C.; Yu, K.; Feng, Y.; Chang, Y.; Yang, T.; Xuan, Y.; Lei, D.; Lou, L.-L.; Liu, S. Novel 3DOM-$SrTiO_3$/Ag/Ag_3PO_4 ternary Z-scheme photocatalysts with remarkably improved activity and durability for contaminant degradation. *Appl. Catal., B* **2017**, *210*, 77−87.
(190) Trench, A. B.; Machado, T. R.; Gouveia, A. F.; Assis, M.; da Trindade, L. G.; Santos, C.; Perrin, A.; Perrin, C.; Oliva, M.; Andrés, J.; Longo, E. Connecting structural, optical, and electronic properties and photocatalytic activity of Ag_3PO_4:Mo complemented by DFT calculations. *Appl. Catal., B* **2018**, *238*, 198−211.
(191) dos Santos, C. C.; de Assis, M.; Machado, T. R.; dos Santos Pereira, P. F.; Minguez-Vega, G.; Cordoncillo, E.; Beltran-Mir, H.; Doñate-Buendía, C.; Andrés, J.; Longo, E. Proof-of-Concept Studies Directed toward the Formation of Metallic Ag Nanostructures from Ag_3PO_4 Induced by Electron Beam and Femtosecond Laser. *Part. Part. Syst. Charact.* **2019**, *36*, 1800533.
(192) Ceroni Galloso, M.; Angulo-Cornejo, J. R.; Lino-Pacheco, M. N.; Villanueva Huerta, C. C.; Casimiro Soriano, E. M. Synthesis and characterization of mixed-ligand silver(I) saccharinate complex containing 2-(2-pyridyl)benzimidazole. *Rev. Colomb. Quim.* **2018**, *47*, 73−78.
(193) Aouadi, S. M.; Schultze, D. M.; Rohde, S. L.; Wong, K.-C.; Mitchell, K. A. R. Growth and characterization of Cr_2N/CrN multilayer coatings. *Surf. Coat. Technol.* **2001**, *140*, 269−277.
(194) Yang, H.; Shang, L.; Zhang, Q.; Shi, R.; Waterhouse, G. I. N.; Gu, L.; Zhang, T. A universal ligand mediated method for large scale synthesis of transition metal single atom catalysts. *Nat. Commun.* **2019**, *10*, 4585.
(195) Bulushev, D. A.; Chuvilin, A. L.; Sobolev, V. I.; Stolyarova, S. G.; Shubin, Y. V.; Asanov, I. P.; Ishchenko, A. V.; Magnani, G.; Riccò, M.; Okotrub, A. V.; Bulusheva, L. G. Copper on carbon materials: stabilization by nitrogen doping. *J. Mater. Chem. A* **2017**, *5*, 10574−10583.
(196) Lyutaya, M. D.; Kulik, O. P. Chemical properties of nitrides of some transition metals. *Powder Metall. Met. Ceram.* **1970**, *9*, 821−826.
(197) Nam, N. D.; Kim, M. J.; Jo, D. S.; Kim, J. G.; Yoon, D. H. Corrosion protection of Ti/TiN, Cr/TiN, Ti/CrN, and Cr/CrN multi-coatings in simulated proton exchange membrane fuel cell environment. *Thin Solid Films* **2013**, *545*, 380−384.
(198) Froment, F. F.; Bischoff, K. B. *Chemical Reactor Analysis and Design*, 2nd ed.; John Wiley: Berlin, 1990.
(199) Butt, J. B. *Reaction Kinetics and Reactor Design*, 2nd ed.; Marcel Dekker: Berlin, 1999.
(200) Serna, P.; Concepción, P.; Corma, A. Design of highly active and chemoselective bimetallic gold−platinum hydrogenation catalysts through kinetic and isotopic studies. *J. Catal.* **2009**, *265*, 19−25.
(201) Millán, R.; Liu, L.; Boronat, M.; Corma, A. A new molecular pathway allows the chemoselective reduction of nitroaromatics on non-noble metal catalysts. *J. Catal.* **2018**, *364*, 19−30.
(202) Bao, X.; Muhler, M.; Pettinger, B.; Schlögl, R.; Ertl, G. On the nature of the active state of silver during catalytic oxidation of methanol. *Catal. Lett.* **1993**, *22*, 215−225.
(203) Waterhouse, G. I. N.; Bowmaker, G. A.; Metson, J. B. Oxygen chemisorption on an electrolytic silver catalyst: a combined TPD and Raman spectroscopic study. *Appl. Surf. Sci.* **2003**, *214*, 36−51.
(204) Cao, E.; Firth, S.; McMillan, P. F.; Gavriilidis, A. Application of microfabricated reactors for operando Raman studies of catalytic oxidation of methanol to formaldehyde on silver. *Catal. Today* **2007**, *126*, 119−126.
(205) Pulido, A.; Concepción, P.; Boronat, M.; Corma, A. Aerobic epoxidation of propene over silver (111) and (100) facet catalysts. *J. Catal.* **2012**, *292*, 138−147.
(206) Shimizu, K.-i.; Kubo, T.; Satsuma, A. Surface Oxygen-Assisted Pd Nanoparticle Catalysis for Selective Oxidation of Silanes to Silanols. *Chem.—Eur. J.* **2012**, *18*, 2226−2229.
(207) Mori, K.; Tano, M.; Mizugaki, T.; Ebitani, K.; Kaneda, K. Efficient heterogeneous oxidation of organosilanes to silanols catalysed by a hydroxyapatite-bound Ru complex in the presence of water and molecular oxygen. *New J. Chem.* **2002**, *26*, 1536−1538.

https://dx.doi.org/10.1021/acssuschemeng.0c08953
ACS Sustainable Chem. Eng. 2021, 9, 2912−2928

(208) Mitsudome, T.; Yamamoto, Y.; Noujima, A.; Mizugaki, T.; Jitsukawa, K.; Kaneda, K. Highly Efficient Etherification of Silanes by Using a Gold Nanoparticle Catalyst: Remarkable Effect of O_2. *Chem.—Eur. J.* **2013**, *19*, 14398−14402.
(209) Urayama, T.; Mitsudome, T.; Maeno, Z.; Mizugaki, T.; Jitsukawa, K.; Kaneda, K. O_2-enhanced Catalytic Activity of Gold Nanoparticles in Selective Oxidation of Hydrosilanes to Silanols. *Chem. Lett.* **2015**, *44*, 1062−1064.
(210) Voronova, E. D.; Golub, I. E.; Pavlov, A.; Belkova, N. V.; Filippov, O. A.; Epstein, L. M.; Shubina, E. S. Dichotomous Si−H Bond Activation by Alkoxide and Alcohol in Base-Catalyzed Dehydrocoupling of Silanes. *Inorg. Chem.* **2020**, *59*, 12240−12251.
(211) Corriu, R. J. P.; Guerin, C.; Henner, B.; Wang, Q. Pentacoordinate hydridosilicates: synthesis and some aspects of their reactivity. *Organometallics* **1991**, *10*, 2297−2303.
(212) Corriu, R.; Guérin, C.; Henner, B.; Wang, Q. Hydridosilicates: a new class of pentacoordinated silicon derivatives with unusual properties. *Inorg. Chim. Acta* **1992**, *198−200*, 705−713.
(213) Chuit, C.; Corriu, R. J. P.; Reye, C.; Young, J. C. Reactivity of penta- and hexacoordinate silicon compounds and their role as reaction intermediates. *Chem. Rev.* **1993**, *93*, 1371−1448.
(214) Lemos, P. S.; Silva, G. S.; Roca, R. A.; Assis, M.; Torres-Mendieta, R.; Beltrán-Mir, H.; Mínguez-Vega, G.; Cordoncillo, E.; Andrés, J.; Longo, E. Laser and electron beam-induced formation of Ag/Cr structures on Ag_2CrO_4. *Phys. Chem. Chem. Phys.* **2019**, *21*, 6101−6111.
(215) Assis, M.; Cordoncillo, E.; Torres-Mendieta, R.; Beltrán-Mir, H.; Mínguez-Vega, G.; Oliveira, R.; Leite, E. R.; Foggi, C. C.; Vergani, C. E.; Longo, E.; Andrés, J. Towards the scale-up of the formation of nanoparticles on α-Ag_2WO_4 with bactericidal properties by femtosecond laser irradiation. *Sci. Rep.* **2018**, *8*, 1884.
(216) de Oliveira, R. C.; de Foggi, C. C.; Teixeira, M. M.; da Silva, M. D. P.; Assis, M.; Francisco, E. M.; Pimentel, B. N. A. d. S.; Pereira, P. F. d. S.; Vergani, C. E.; Machado, A. L.; Andres, J.; Gracia, L.; Longo, E. Mechanism of Antibacterial Activity via Morphology Change of α-$AgVO_3$: Theoretical and Experimental Insights. *ACS Appl. Mater. Interfaces* **2017**, *9*, 11472−11481.

https://dx.doi.org/10.1021/acssuschemeng.0c08953
ACS Sustainable Chem. Eng. 2021, 9, 2912−2928